



Title :

ORCHIDEE MICT-LEAK (r5459), a global model for the production, transport and transformation of dissolved organic carbon from Arctic permafrost regions, Part 1: Rationale, model description and simulation protocol.

Authors:

Simon P.K. Bowring¹, Ronny Lauerwald², Bertrand Guenet¹, Dan Zhu¹, Matthieu Guimberteau^{1,3}, Ardalan Tootchi³, Agnès Ducharne³, Philippe Ciais¹

Affiliations:

[1] Laboratoire des Sciences du Climat et de l'Environnement, LSCE, CEA, CNRS, UVSQ, 91191 Gif Sur Yvette, France

[2] Department of Geoscience, Environment & Society, Université Libre de Bruxelles, 1050 Bruxelles, Belgium

[3] Sorbonne Université, CNRS, EPHE, Milieux environnementaux, transferts et interaction dans les hydrosystèmes et les sols, Metis, 75005 Paris, France

Abstract

Few Earth System models adequately represent the unique permafrost soil biogeochemistry and its respective processes; this significantly contributes to uncertainty in estimating their responses, and that of the planet at large, to warming. Likewise, the riverine component of what is known as the 'boundless carbon cycle' is seldom recognized in Earth System modeling. Hydrological mobilization of organic material from a ~1330–1580 PgC carbon stock to the river network results either in sedimentary settling or atmospheric 'evasion', processes widely expected to increase with amplified Arctic climate warming. Here, the production, transport and atmospheric release of dissolved organic carbon (DOC) from high-latitude permafrost soils into inland waters and the ocean is explicitly represented for the first time in the land surface component (ORCHIDEE) of a CMIP6 global climate model (IPSL). The model, ORCHIDEE MICT-LEAK, mechanistically represents (a) vegetation and soil physical processes for high latitude snow, ice and soil phenomena, and (b) the cycling of DOC and CO₂, including atmospheric evasion, along the terrestrial-aquatic continuum from soils through the river network to the coast, at 0.5° to 2° resolution. This paper, the first in a two-part study, presents the rationale for including these processes in a high latitude specific land surface model, then describes the model with a focus on novel process implementations, followed by a summary of the model configuration and simulation protocol. The results of these simulation runs, conducted for the Lena River basin, are evaluated against observational data in the second part of this study.

1 Introduction

High-latitude permafrost soils contain large stores of frozen, often ancient and relatively reactive carbon up to depths of over 30m. Soil warming caused by contemporary anthropogenic climate change can be expected to destabilize these stores (Schuur et al., 2015) via microbial or hydrological mobilization following spring/summer thaw and riverine discharge (Vonk et al., 2015a) as the permafrost line migrates poleward over time. The high latitude soil carbon reservoir may amount to ~1330–1580 PgC (Hugelius et al., 2013, 2014; Tarnocai et al., 2009) –over double that stored in the contemporary atmosphere, while the yearly lateral flux of carbon from soils to running waters may



50 amount to ~40% of net ecosystem carbon exchange (McGuire et al., 2009), the majority
51 as dissolved organic carbon (DOC).

52
53 The fact that, to our knowledge, no existing land surface models are able to adequately
54 simultaneously represent this unique high latitude permafrost soil environment, the
55 transformation of soil organic carbon (SOC) to its eroded particulate and DOC forms and
56 their subsequent lateral transport, as well as the response of all these to warming,
57 entails significant additional uncertainty in projecting global-scale biogeochemical
58 responses to human-induced environmental change.

59
60 Fundamental to these efforts is the ability to predict the medium under which carbon
61 transformation will occur: in the soil, streams, rivers or sea, and under what
62 metabolising conditions –since these will determine the process mix that will ultimately
63 enable either terrestrial redeposition and retention, ocean transfer, or atmospheric
64 release of permafrost-derived organic carbon. In the permafrost context, this implies
65 being able to accurately represent (i) the source, reactivity and transformation of
66 released organic matter, and; (ii) the dynamic response of hydrological processes to
67 warming, since water phase determines carbon, heat, and soil moisture availability for
68 metabolism and lateral transport.

69
70 To this end, we take a specific version of the terrestrial component of the IPSL global
71 Earth System model (ESM) ORCHIDEE (Organising Carbon and Hydrology In Dynamic
72 Ecosystems), one that is specifically coded for, calibrated with and evaluated on high
73 latitude phenomena and permafrost processes, called ORCHIDEE-MICT (Guimberteau et
74 al., 2018). This code is then adapted to include DOC production in the soil (ORCHIDEE-
75 SOM, (Camino-Serrano et al., 2018)), ‘priming’ of SOC (ORCHIDEE-PRIM, (Guenet et al.,
76 2016, 2018)) and the riverine transport of DOC and CO₂, including in-stream
77 transformations, carbon and water exchanges with wetland soils and gaseous exchange
78 between river surfaces and the atmosphere (ORCHILEAK, (Lauerwald et al., 2017)).

79
80 The resulting model, dubbed ORCHIDEE MICT-LEAK, hereafter referred to as MICT-L for
81 brevity, is therefore able to represent: (a) Permafrost soil and snow physics,
82 thermodynamics to a depth of 38m and dynamic soil hydrology to a depth of 2m; (b)
83 Improved representation of biotic stress response to cold, heat and moisture in high
84 latitudes; (c) Explicit representation of the active layer and frozen-soil hydrologic
85 barriers; buildup of soil carbon stocks via primary production and vertical translocation
86 (turbation) of SOC and DOC; (d) DOC leaching from tree canopies, atmospheric
87 deposition, litter and soil organic matter, its adsorption/desorption to/from soil
88 particles, its transport and transformation to dissolved CO₂ (CO_{2(aq.)}) and atmospheric
89 release, as well as the production and hydrological transport of plant root-zone derived
90 dissolved CO₂; (e) Improved representation of C cycling on floodplains; (f) Priming of
91 organic matter in the soil column and subsequent decomposition dynamics. In
92 combination, these model properties allow us to explore the possibility of reproducing
93 important emergent phenomena observed in recent empirical studies (Fig. 1) arising
94 from the interaction of a broad combination of different processes and factors.

95
96 To our knowledge very few attempts have been made at the global scale of modelling
97 DOC production and lateral transfer from the permafrost region that explicitly accounts
98 for such a broad range of high latitude-specific processes, which in turn allows us to



match and evaluate simulation outputs with specific observed processes, enhancing our ability to interpret the output from these models and improve our understanding of the processes represented. The only other attempt at doing so is a Pan-Arctic modelling study by Kicklighter et al. (2013), which is based on a relatively simplified scheme for soil, water and biology. The following segment briefly overviews the dynamics, emergent properties and their overall significance across scales, of permafrost region river basins.

A giant, reactive, fast-draining funnel: A permafrost basin overview

Permafrost has a profound impact on Arctic river hydrology. In permafrost regions, a permanently frozen soil layer acts as a ‘cap’ on ground water flow (see ‘permafrost barrier’, right hand side of Fig. 1). This implies that: (i) Near-surface runoff becomes by far the dominant flowpath draining permafrost watersheds (Ye et al., 2009), as shown in Fig. 1d; (ii) The seasonal amplitude of river discharge, expressed by the ratio of maximum to minimum discharge ($Q_{\max:\min}$ in Fig. 1), over continuous versus discontinuous permafrost catchments is higher as a result of the permafrost barrier; (iii) This concentration of water volume near the surface causes intense leaching of DOC from litter and relevant unfrozen soil layers (Fig. 1g, 1d, e.g. Drake et al., (2015); Spencer et al., (2015); (Vonk et al., (2015a,b)); (iv) Permafrost SOC stocks beneath the active layer are physically and thermally shielded from aquatic mobilization and metabolization, respectively (Fig. 1g).

Rapid melting of snow and soil or river ice during spring freshet (May-June) drives intensely seasonal discharge, with peaks often two orders of magnitude (e.g. Van Vliet et al., (2012)) above baseflow rates (Fig. 1d). These events are the cause of four, largely synchronous processes: (i) Biogenic matter is rapidly transported from elevated headwater catchments (Fig. 1, right hand side) (McClelland et al., 2016); (ii) Plant material at the soil surface is intensely leached, with subsequent mobilization and transformation of this dissolved matter via inland waters (Fig. 1d,b,j); During spring freshet, riverine DOC concentrations increase and bulk annual marine DOC exports are dominated by the terrestrial DOC flux to the rivers that occurs at this time (Holmes et al., 2012). Indeed, DOC concentrations during the thawing season tend to be greater than or equal to those in the Amazon particularly in the flatter Eurasian rivers (Holmes et al., 2012; McClelland et al., 2012), and DOC concentrations are affected at watershed scale by parent material and ground ice content (O'Donnell et al., 2016).

(iii) Sudden inundation of the floodplain regions in spring and early summer (Fig. 1h), (Smith and Pavelsky, 2008), further spurs lateral flux of both particulate and dissolved matter in the process and its re-deposition (Zubrzycki et al., 2013) or atmospheric evasion (Fig. 1j,m); (iv) Snowmelt-induced soil water saturation, favoring the growth of moss and sedge-based ecosystems (e.g. Selvam et al., 2017; Tarnocai et al., 2009; Yu, 2011) and the retention of their organic matter (OM), i.e., peat formation, not shown in Fig. 1 as this isn't represented in this model version, but is generated in a separate branch of ORCHIDEE (Qiu et al., 2018)).

Mid-summer river low-flow and a deeper active layer allow for the hydrological intrusion and leaching of older soil horizons (e.g. the top part of Pleistocene-era Yedoma soils), and their subsequent dissolved transport (e.g. Wickland et al., 2018). These



148 sometimes-ancient low molecular weight carbon compounds appear to be preferentially
149 and rapidly metabolized by microbes in headwater streams (Fig. 1j), which may
150 constitute a significant fraction of aggregate summer CO₂ evasion in Arctic rivers
151 (Denfeld et al., 2013; Vonk et al., 2015). This is likely due to the existence of a significant
152 labile component of frozen carbon (Drake et al., 2015; Vonk et al., 2013; Woods et al.,
153 2011);

154
155 CO₂ evasion rates from Arctic inland waters (Fig. 1j,e,m) are estimated to be in the
156 region of 40-84 TgC yr⁻¹ (McGuire et al., 2009), to be compared with estimates of Pan
157 Arctic DOC discharge from rivers of 25-36 TgC yr⁻¹. The influx of terrestrial carbon to
158 the shelf zone is thought to total 45-54 TgC yr⁻¹ (Holmes et al., 2012; Raymond et al.,
159 2007). Rivers supply the Arctic Ocean (AO) an estimated 34 Tg DOC-C yr⁻¹ (Holmes et al.,
160 2012), while depositing 5.8 Tg yr⁻¹ of particulate carbon, these being sourced from those
161 rivers draining low and high elevation headwaters, respectively (McClelland et al.,
162 2016). These dynamics are all subject to considerable amplification by changes in
163 temperature and hydrology (e.g. Frey et al., 2009; Drake et al., 2015; Tank et al., 2018).

164
165 Average annual discharge in the Eurasian Arctic rivers has increased by at least 7%
166 between 1936-1999 (Peterson et al., 2002), driven by increasing temperatures and
167 runoff (Berezovskaya et al., 2005), and the subsequent interplay of increasing annual
168 precipitation, decreasing snow depth and snow water equivalent (SWE) mass (Kunkel et
169 al., 2016; Mudryk et al., 2015), and greater evapotranspiration (Zhang et al., 2009).
170 Although net discharge trend rates over N. America were negative over the period 1964-
171 2003, since 2003 they have been positive on average (Dery et al., 2016). These dynamic
172 and largely increasing hydrologic flux trends point towards temperature and
173 precipitation -driven changes in the soil column, in which increased soil water/snow
174 thaw and microbial activity (Graham et al., 2012; MacKelprang et al., 2011; Schuur et al.,
175 2009) converge to raise soil leaching and DOC export rates to the river basin and beyond
176 (e.g. Vonk et al., (2015b)). Further, microbial activity generates its own heat, which
177 incubation experiments have shown may be sufficient to significantly warm the soil
178 further (Hollesen et al., 2015), in a positive feedback.

179
180 Arctic region fire events are also on the rise and likely to increase with temperature and
181 severity over time (Ponomarev et al., 2016). The initial burning of biomass is
182 accompanied by active layer deepening, priming of deeper soil horizons (De Baets et al.,
183 2016), and a significant loading of pyrogenic DOC in Arctic watersheds, up to half of
184 which is rapidly metabolized (Myers-Pigg et al., 2015).

185
186 In these contexts, the implications of (polar-amplified) warmer temperatures leading to
187 active layer deepening towards the future (transition from Continuous to Discontinuous
188 Permafrost, as shown in the upper/lower segments of Fig. 1) are clear and unique:
189 potentially sizeable aquatic mobilization and microbial metabolism (Xue, 2017) of
190 dissolved and eroded OM, deeper hydrological flow paths, an increase in total carbon
191 and water mass and heat transfer to the aquatic network and, ultimately, the Arctic
192 Ocean and atmosphere (Fig. 1i).

193
194 The advantage of having a terrestrial model that can be coupled to a marine component
195 of an overarching global climate model (GCM) is in this case the representation of a
196 consistent transboundary scheme, such that output from one model is integrated as



input to another. This is particularly important given the context in which these terrestrial outflows occur :

Because of its small size, a uniquely large and shallow continental shelf, the global climatological significance of its seasonal sea ice (Rhein et al., 2013) and its rapid decline (Findlay et al., 2015), the AO has been described as a giant estuary (McClelland et al., 2012), acting as a funnel for the transport, processing and sedimentation of terrestrial OM. Because of its small surface area and shallow seas (Jakobsson, 2002), the AO holds relatively little volume and is consequently sensitive to inputs of freshwater, heat, alkalinity and nutrients that flush out from terrestrial sources, particularly at discharge peak.

High suspended particle loads in river water as they approach the mouth (Heim et al., 2014) cause lower light availability and water albedo and hence higher temperatures (Bauch et al., 2013; Janout et al., 2016), which can affect the near-shore sea ice extent, particularly in spring (Steele and Ermold, 2015). Volumes of riverine freshwater and total energy flux (Lammers et al., 2007) are expected to increase with warmer temperatures, along with an earlier discharge peak (Van Vliet et al., 2012, 2013). In doing so, freshwaters may in the future trigger earlier onset of ice retreat (Stroeve et al., 2014; Whitefield et al., 2015) via a freshwater albedo, ice melt, seawater albedo, ice melt, feedback, amplified by intermediary state variables such as water vapor and cloudiness (Serreze and Barry, 2011).

Both terrestrially-exported and older shelf carbon in the AO face considerable disruption (McGuire et al., 2009; Schuur et al., 2015) from the combined effects of increased freshwater, heat, sediment, nutrient and organic carbon flows from rapidly warming Arctic river watersheds, as well as those from melting sea ice, warmer marine water temperatures and geothermal heat sources (Janout et al., 2016; Shakhova et al., 2015). Because ORCHIDEE is a sub-component of the overarching IPSL ESM, there is scope for coupling riverine outputs of water, DOC, $\text{CO}_{2(\text{aq})}$ and heat from the terrestrial model as input for the IPSL marine components (Fig. 1i). Nonetheless, these are not the objectives of the present paper, whose aim is rather to validate the simulated variable output produced by the model described in detail below against observations and empirical knowledge for the Lena basin, but are included here descriptively to scope the plausible future applications of ORCHIDEE MICT-LEAK, given our present empirical understanding of their potential significance.

The Methods section summarises the model structure and associated rationale for each of the model sub-branches or routines relevant to this study, and follows with the setup and rationale for the simulations carried out as validation exercises.

2 Methods

This section overviews the processes represented in the model being described in this manuscript, which is referred to as ORCHIDEE MICT-LEAK, hereafter referred to MICT-L for brevity. MICT-L is at its heart a merge of two distinct models : the high-latitude land surface component of the IPSL Earth System Model ORCHIDEE MICT, and the DOC-production and transport branch of ORCHIDEE's default or 'trunk' version (Krinner et al., 2005), ORCHILEAK. The original merger of these two code sets was between



ORCHILEAK and ORCHIDEE-MICT, which are described in Camino-Serrano et al. (2018)/Lauerwald et al. (2017) and Guimberteau et al. (2018), respectively.

However, numerous bug fixes and process additions post-dating these publications have been included in this code. Furthermore, novel processes included in neither of these two core models are added to MICT-L in response to phenomena reported in recent empirical publications, such as the diffusion of DOC (novel in ORCHIDEE-MICT) through the soil column to represent its turbation and preferential stabilisation at depth in the soil, in a process not necessarily the same as its adsorption –also represented here.

In terms of code architecture, the resulting model is substantially different from either of its parents, owing to the fact that the two models were developed on the basis of ORCHIDEE trunk revisions 2728 and 3976 for ORCHILEAK and MICT respectively, which have a temporal model development distance of over 2 years, and subsequently evolved in their own directions. These foundational differences, which mostly affect the formulation of soil, carbon and hydrology schemes, mean that different aspects of each are necessarily forced into the subsequent code. Where these differences were considered scientific or code improvements, they were included in the resulting scheme.

Where these differences were so large as to prove a burden in excess of the scope of this first model version, such as the inclusion of the soil carbon spinup module, they were omitted from this first revision of MICT-L. The direction of the merge –which model was the base which incorporated code from the other –was from ORCHILEAK into MICT, given that the latter contains the bulk of the fundamental (high latitude) processes necessary for this merge. Despite architectural novelties introduced, MICT-L carries with it a marriage of much the same schemes detailed exhaustively in Guimberteau et al. (2018) and Lauerwald et al. (2017). As such, the following model description details only new elements of the model, those that are critical to the production and transport of DOC from permafrost regions, and parameterisations specific to this study (Fig. 2).

2.1 Model Description

MICT-L is based largely on ORCHIDEE-MICT, into which the DOC production, transport and transformation processes developed in the ORCHILEAK model version and tested insofar only for the Amazon, have been transplanted, allowing for these same processes to be generated in high latitude regions with permafrost soils and a river flow regime dominated by snow melt. The description that ensues roughly follows the order of the carbon and water flow chain depicted in Fig. 2b. At the heart of the scheme is the vegetative production of carbon, which occurs along a spectrum of 13 plant functional types (PFTs) that differ from one another in terms of plant physiological and phenological uptake and release parameters (Krinner et al., 2005). Together, these determine grid-scale net primary production. In the northern high latitudes, the boreal trees (PFTs 7-9) and C3 grasses (PFT 10) dominate landscape biomass and primary production. Thus, in descending order yearly primary production over the Lena basin is roughly broken down between C3 grasses (48%), boreal needleleaf summergreen trees (27%), boreal needleleaf evergreen trees (12%), boreal broadleaf summergreen trees (8%) and temperate broad-leaved evergreen trees (6%). Naturally these basin aggregates are heterogeneously distributed along latitude and temperature contours, with grasses/tundra dominating at the high latitudes and (e.g.) temperate broadleaf



trees existing only at the southern edges of the basin.

2.2 Biomass generation (Fig. 1a)

Biomass generation, consisting of foliage, roots, above and below –ground sap and heart wood, carbon reserves and fruit pools in the model, results in the transfer of these carbon stores to two downstream litter pools, the structural and metabolic litter (Figure 2b). This distinction, defined by lignin concentration of each biomass pool (Krinner et al., 2005), separates the relatively reactive litter fraction such as leafy matter from its less-reactive, recalcitrant counterpart (woody, ‘structural’ material), with the consequence that the turnover time of the latter is roughly four-fold that of the former. These two litterpools are further subdivided into above and below –ground pools, with the latter explicitly discretised over the first two metres of the soil column, a feature first introduced to the ORCHIDEE model by Camino-Serrano et al. (2014, 2018). This marks a significant departure from the original litter formulation in ORCHIDEE-MICT, in which the vertical distribution of litter influx to the soil carbon pool follows a prescribed root profile for each PFT. This change now allows for the production of DOC from litter explicitly at a given soil depth in permafrost soils.

2.3 DOC generation and leaching (Fig. 1b)

The vast majority of DOC produced by the model is generated initially from the litter pools via decomposition, such that half of all of the decomposed litter is returned to the atmosphere as CO₂, as defined by the microbial carbon use efficiency (CUE) –the fraction of carbon assimilated versus respired by microbes post-consumption –here set at 0.5 following Manzoni et al. (2012). The non-respired half of the litter feeds into ‘Active’, ‘Slow’ and ‘Passive’ free DOC pools, which correspond to DOC reactivity classes in the soil column. Metabolic litter contributes exclusively to the Active DOC pool, while Structural litter feeds into the other two, the distribution between them dependent on the lignin content of the Structural litter. The reactive SOC pools then derive directly from this DOC reservoir, in that fractions of each DOC pool, defined again by the CUE, are directly transferred to three different SOC pools, while the remainder adds to the heterotrophic soil respiration. Depending on clay content and bulk density of the soil, a fraction of DOC is adsorbed to the mineral soil and does not take part in these reactions until it is gradually desorbed when concentrations of free DOC decrease in the soil column. This scheme is explained in detail in Camino-Serrano (2018). The value of the fractional redistributions between free DOC and SOC after adsorption are shown in Fig. 2b.

The approximate ratio of relative residence times for the three SOC pools in our model (Active :Slow :Passive) is (1 :37:1618) at a soil temperature of 5°C, or 0.843 years, 31 yrs. and 1364 yrs. for the three pools respectively (Fig. 2b). These are based on our own exploratory model runs and subsequent calculations. The residence times of the active DOC pool is ~7 days (0.02 yrs.), while the slow and passive DOC pools both have a residence time of ~343 days (0.94 yrs.) at that same temperature. Upon microbial degradation in the model, SOC of each pool reverts either to DOC or to CO₂, the ratio between these determined again by the CUE which is set in this study at 0.5 for all donor pools, in keeping with the parameter configuration in Lauerwald et al., (2017) from Manzoni et al. (2012). This step in the chain of flows effectively represents leaching of



SOC to DOC. Note that the reversion of SOC to DOC occurs only along Active-Active, Slow-Slow and Passive-Passive lines in Fig. 2b, while the conversion of DOC to SOC is distributed differently so as to build up a reasonable distribution of soil carbon stock reactivities. Note also that the microbial CUE is invoked twice in the chain of carbon breakdown, meaning that the 'effective' CUE of the SOC-litter system is approximately 0.25.

2.4 Throughfall and its DOC (Fig. 1c)

In MICT-L, DOC generation also occurs in the form of wet and dry atmospheric deposition and canopy exudation, collectively attributed to the throughfall, i.e. the amount of precipitation reaching the ground. Wet atmospheric deposition originates from organic compounds dispersed in atmospheric moisture which become deposited within rainfall, and are assumed here to maintain a constant concentration. This concentration we take from the average of reported rainfall DOC concentrations in the empirical literature measured at sites >55°N (Bergkvist and Folkeson, 1992; Clarke et al., 2007; Fröberg et al., 2006; Lindroos et al., 2011; Rosenqvist et al., 2010; Starr et al., 2003; Wu et al., 2010), whose value is 3 mgC L⁻¹ of rainfall. Dry DOC deposition occurs through aerosol-bound organic compounds, here assumed to fall on the canopy; canopy exudation refers to plant sugars exuded from the leaf surface (e.g. honey dew) or from their extraction by heterotrophs such as aphids. These two are lumped together in our estimates of canopy DOC generation (gDOC per g leaf carbon), which is calibrated as follows.

We take the average total observation-based throughfall DOC flux rate per m² of forest from the aforementioned literature bundle (15.7 gC m⁻² yr⁻¹) and subtract from it the wet deposition component (product of rainfall over our simulation area and the rain DOC content). The remainder is then the canopy DOC, which we scale to the average leaf biomass simulated in a 107-year calibration run over the Lena river basin, to obtain a constant, non-conservative canopy DOC production rate of 9.2*10⁻⁴ g DOC-C per gram leaf biomass per day (Eq. 1), except for the crop PFTs for which this value equals 0. Note that this production of DOC should be C initially fixed by photosynthesis, but it is here represented as an additional carbon flux. The dry deposition of DOC through the canopy is given by:

$$(1) \text{TF}_{\text{DRY}} = M_{\text{LEAF}} * 9.2 * 10^{-4} \frac{dt}{\text{day}}$$

Where TF_{DRY} is dry deposition of DOC from the canopy, M_{LEAF} is leaf biomass, dt is the timestep of the surface hydrology and energy balance module (30min) and day is 24 hours. This accumulates in the canopy and can be flushed out with the throughfall and percolates into the soil surface or adds to the DOC stock of surface waters. The wet and canopy deposition which hits the soil is then assumed to be split evenly between the labile and refractory DOC pools (following Aitkenhead-Peterson et al., 2003).

2.5 Hydrological mobilisation of soil DOC (Fig. 1d)



390 All DOC pools, leached from the decomposition of either litter and SOC or being
391 throughfall inputs, reside at this point in discrete layers within the soil column, but are
392 now also available for vertical advection and diffusion, as well as lateral export from the
393 soil column as a carbon tracer, via soil drainage and runoff.

394
395 Export of DOC from the soil to rivers occurs through surface runoff, soil-bottom
396 drainage, or flooding events (see sections ‘soil flooding’ and ‘floodplain representation’).
397 Runoff is activated when the maximum water infiltration rate of the specific soil has
398 been exceeded, meaning that water arrives at the soil surface faster than it can enter,
399 forcing it to be transported laterally across the surface. DOC is drawn up into this
400 runoff water flux from the first 5 layers of the soil column, which correspond to a
401 cumulative source depth of 4.5cm.

402
403 Drainage of DOC occurs first as its advection between the discrete soil layers, and its
404 subsequent export from the 11th layer, which represents the bottom of the first 2m of
405 the soil column, from which export is calculated as a proportion of the DOC
406 concentration at this layer. Below this, soil moisture and DOC concentrations are no
407 longer explicitly calculated, except in the case that they are cryoturbated below this, up
408 to a depth of 3m. DOC drainage is proportional to but not a constant multiplier of the
409 water drainage rate for two reasons. First, in the process of drainage DOC is able to
410 percolate from one layer to another, through the entirety of the soil column, meaning
411 that vertical transport is not solely determined by 11th layer concentrations, given that
412 DOC can be continuously leached and transported over the whole soil column. Secondly,
413 in order to account for preferential flow paths in the soil created by the subsoil actions
414 of flora and fauna, and for the existence of non-homogenous soil textures at depth that
415 act as aquitards, DOC infiltration must account for the fact that area-aggregated soils
416 drain more slowly, increasing the residence time of DOC in the soil. Thus a reduction
417 factor which reduces the vertical advection of DOC in soil solution by 80% compared to
418 the advection is applied to represent a slow down in DOC percolation through the soil
419 and increase its residence time there.

420
421 In MICT-L, as in ORCHILEAK, a ‘poor soils’ module reads off from a map giving fractional
422 coverage of land underlain by Podzols and Arenosols at the 0.5° grid-scale, as derived
423 from the Harmonized World Soil Database (Nachtergaele, 2010). Due to their low pH
424 and nutrient levels, areas identified by this soil-type criterion experience soil organic
425 matter decomposition rates half that of other soils (Lauerwald et al. (2017), derived
426 from Bardy et al. (2011); Vitousek & Sanford (1986); Vitousek & Hobbie (2000)). To
427 account for the very low DOC-filtering capacity of these coarse-grained, base- and clay-
428 poor soils (DeLuca & Boisvenue (2012), Fig. 2b), no reduction factor in DOC advection
429 rate relative to that of water in the soil column is applied when DOC is generated within
430 these “poor soils”.

431
432 By regulating both decomposition and soil moisture flux, the “poor soil” criterion
433 effectively serves a similar if not equal function to a soil ‘tile’ for DOC infiltration in the
434 soil column (inset box of Fig. 1), because soil tiles (forest, grassland/tundra/cropland
435 and bare soil) are determinants of soil hydrology which affects moisture-limited
436 decomposition. Here however, the ‘poor soil’ criteria is applied uniformly across the
437 three soil tiles of each grid cell. This modulation in MICT-L is of significance for the
438 Arctic region, given that large fractions of the discontinuous permafrost region are



underlain by Podzols, particularly in Eurasia. For the Arctic as a whole, Podzols cover ~15% of total surface area (DeLuca and Boisvenue, 2012). Further, in modelled frozen soils, a sharp decline in hydraulic conductivity is imposed by the physical barrier of ice, which retards the flow of water to depth in the soil, imposing a cap on drainage and thus potentially increasing runoff of water laterally, across the soil surface (Gouttevin et al., 2012). In doing so, frozen soil layers overlain by liquid soil moisture will experience enhanced residence times of water in the carbon-rich upper soil layers, potentially enriching their DOC load.

Thus, for all the soil layers in the first 2m, DOC stocks are controlled by production from litter and SOC decay, their advection, diffusion, and consumption by DOC mineralization, as well as buffering by adsorption and desorption processes.

2.6 Routing Scheme:

The routing scheme in ORCHIDEE, first described in detail in Ngo-Duc et al. (2007) and presented after some version iterations in Guimberteau et al. (2012), is the module which when activated, represents the transport of water collected by the runoff and drainage simulated by the model along the prescribed river network in a given watershed. In doing so, its purpose is to coarsely represent the hydrologic coupling between precipitation inputs to the model and subsequent terrestrial runoff and drainage (or evaporation) calculated by it on the one hand, and the eventual discharge of freshwater to the marine domain, on the other. In other words, the routing scheme simulates the transport of water by rivers and streams, by connecting rainfall and continental river discharge with the land surface.

To do so, the routing scheme first inputs a map of global watersheds at the 0.5 degree scale (Oki et al., 1999; Vorosmarty et al., 2000) which gives watershed and sub-basin boundaries and the direction of water-flow based on topography to the model. The water flows themselves are comprised of three distinct linear reservoirs within each sub-basin ('slow', 'fast', 'stream'). Each water reservoir is represented at the subgrid scale (here: 4 subgrid units per grid cell), and updated with the lateral in- and outflows at a daily time-step. The 'slow' water reservoir aggregates the soil drainage, i.e. the vertical outflow from the 11th layer (2 m depth) of the soil column, effectively representing the 'shallow groundwater' storage. The 'fast' water reservoir aggregates surface runoff simulated in the model, effectively representing overland hydrologic flow. The 'slow' and 'fast' water reservoirs feed a delayed outflow to the 'stream' reservoir of the adjacent subgrid-unit in the downstream direction.

The water residence time in each reservoir depends on the nature of the reservoir (increasing residence time in the order : stream < fast < slow reservoir). More generally, residence time decreases with the steepness of topography, given by the product of a local topographic index and a constant with decreasing values for the 'slow', 'fast' and 'stream' reservoirs. The topographic index is the ratio of the grid-cell length to the square root of the mean slope, to reproduce the effect of geomorphological factors in Manning's equation (Ducharne et al., 2003; Guimberteau et al., 2012; Manning, 1891) and determines the time that water and DOC remain in soils prior to entering the river network. In this way the runoff and drainage are exported from sub-unit to sub-unit and from grid-cell to grid-cell.



2.7 Grid-scale water and carbon routing (Fig. 1f, 1g)

Water-borne, terrestrially-derived DOC and dissolved CO₂ in the soil solution are exported over the land surface using the same routing scheme. When exported from soil or litter, DOC remains differentiated in the numerical simulations according to its initial reactivity within the soil (Active, Slow, Passive). However, because the terrestrial Slow and Passive DOC pools (Camino-Serrano et al., 2018) are given the same residence time, these two pools are merged when exported (Lauerwald et al., 2017): Active DOC flows into a Labile DOC hydrological export pool, while the Slow and Passive DOC pools flow into a Refractory DOC hydrological pool (Fig. 2b). The water residence times in each reservoir of each subgrid-unit determine the decomposition of DOC into CO₂ within water reservoirs, before non-decomposed DOC is passed on to the next reservoir downstream.

The river routing calculations, which occur at a daily timestep, are then aggregated to one-day for the lateral transfer of water, CO_{2(aq)} and DOC from upstream grid to downstream grid according to the river network. Note that carbonate chemistry in rivers and total alkalinity routing are not calculated here.

In this framework, the ‘fast’ and ‘slow’ residence times of the water pools in the routing scheme determine the time that water and DOC remains in overland and groundwater flow before entering the river network. Note that while we do not explicitly simulate headwater streams as they exist in a geographically determinant way in the real world, we do simulate what happens to the water before it flows into a river large enough to be represented in the routing scheme by the water pool called ‘stream’. The ‘fast’ reservoir, which is indicative of the pool of runoff water that is destined for entering the ‘stream’ water reservoir, is implicitly representative of headwater streams non resolved by the model routing as an explicit stream pool at a given spatial resolution, as it fills the spatial and temporal niche between runoff and the river stem. The dynamics of headwater hydrological and DOC dynamics (Section 2.10) are of potentially great significance with respect to carbon processing, as headwater catchments have been shown to be ‘hotspots’ of carbon metabolism and outgassing in Arctic rivers, despite their relatively small areal fraction (Denfeld et al., 2013; Drake et al., 2015; Mann et al., 2015; Venkiteswaran et al., 2014; Vonk et al., 2013, 2015a, 2015b). Thus, in what follows in this study, we refer to what in the code are called the ‘fast’ and ‘stream’ pools, which represent the small streams and large stream or river pools, respectively, using ‘stream’ and ‘river’ to denote these from hereon in.

Furthermore, the differentiated representation of water pools as well as mean grid cell slope, combined with the dynamic active layer simulated for continuous versus discontinuous permafrost, is important for reproducing the phenomena observed by Kutscher et al. (2017) and Zhang et al. (2017) for sloping land as shown on the right hand side of Fig. 1. In discontinuous permafrost and permafrost free regions, these phenomena encompass landscape processes (sub-grid in the model), through which water flow is able to re-infiltrate the soil column and so leach more refractory DOC deeper in the soil column, leading to a more refractory signal in the drainage waters. In contrast, in continuous permafrost region, the shallow active layer will inhibit the downward re-infiltration flux of water and encourage leaching at the more organic-rich and labile surface soil layer, resulting in a more labile DOC signal from the drainage in



these areas (Fig. 1). These re-infiltration processes are thought to be accentuated in areas with higher topographic relief (Jasechko et al., 2016), which is why they are represented on sloping areas in Fig. 1.

2.8 Representation of floodplain hydrology and their DOC budget (Fig. 1e,1h)

The third terrestrial DOC export pathway in MICT-L is through flooding of floodplains, a transient period that occurs when stream water is forced by high discharge rates over the river 'banks' and flows onto a flat floodplain area of the grid cell that the river crosses, thus inundating the soil. Such a floodplain area is represented as a fraction of a grid-cell with the maximum extent of inundation, termed the 'potential flooded area' being predefined from a forcing file (Tootchi et al., 2019). Here, the DOC pools that are already being produced in these inundated areas from litter and SOC decomposition in the first 5 layers of the soil column are directly absorbed by the overlying flood waters. These flood waters may then either process the DOC directly, via oxidation to CO₂, (Sections 2.10, 2.11) or return them to the river network, as floodwaters recede to the river main stem, at which point they join the runoff and drainage export flows from upstream.

MICT-L includes the floodplain hydrology part of the routing scheme (D'Orgeval et al., 2008; Guimberteau et al., 2012), as well as additions and improvements described in Lauerwald et al. (2017). The spatial areas that are available for potential flooding are pre-defined by an input map originally based on the map of Prigent et al. (2007). However, for this study, we used an alternative map of the "regularly flooded areas" derived from the method described in Tootchi et al., (2018), which in this study uses an improved input potential flooding area forcing file specific to the Lena basin, that combines three high-resolution surface water and inundation datasets derived from satellite imagery: GIEMS-D15 (Fluet-Chouinard et al., 2015), which results from the downscaling of the map of Prigent et al. (2007) at 15-arc-sec (ca 500 m at Equator); ESA-CCI land cover (at 300 m ~ 10 arc-sec); and JRC surface water at 1 arc-sec (Pekel et al., 2016). The 'fusion' approach followed by this forcing dataset stems from the assumption that the potential flooding areas identified by the different datasets are all valid despite their uncertainties, although none of them is exhaustive. The resulting map was constructed globally at the 15 arc-sec resolution and care was taken to exclude large permanent lakes from the potential flooding area based on the HydroLAKES database (Messenger et al., 2016). In the Lena river basin, the basin against which we evaluate ORCHIDEE MICT-LEAK in Part 2 of this study, this new potential floodplains file gives a maximum floodable area of 12.1% (2.4×10^5 km²) of the 2.5×10^6 km² basin, substantially higher than previous estimates of 4.2% by Prigent et al. (2007).

With this improved forcing, river discharge becomes available to flood a specific pre-defined floodplain grid fraction, creating a temporary floodplains hydrologic reservoir, whose magnitude is defined by the excess of discharge at that point over a threshold value, given by the median simulated water storage of water in each grid cell over a 30 year period. The maximum extent of within-grid flooding is given by another threshold, the calculated height of flood waters beyond which it is assumed that the entire grid is inundated. This height, which used to be fixed at 2 m, is now determined by the 90th percentile of all flood water height levels calculated per grid cell from total water storage of that grid cell over a reference simulation period for the Lena basin, using the



same methodology introduced by Lauerwald et al. (2017). The residence time of water on the floodplains (τ_{flood}) is a determinant of its resulting DOC concentration, since during this period it appropriates all DOC produced by the top 5 layers of the soil column.

2.9 Oceanic outflow (Fig. 1i)

Routing of water and DOC through the river network ultimately lead to their export from the terrestrial system at the river mouth (Fig. 1), which for high latitude rivers are almost entirely sub-deltas of the greater 'estuary', described by McClelland et al. (2012), draining into the Arctic Ocean. Otherwise, the only other loss pathway for carbon export once in the river network is through its decomposition to CO_2 and subsequent escape to the atmosphere from the river surface. DOC decomposition is ascribed a constant fraction for the labile and refractory DOC pools of 0.3 d^{-1} and 0.01 d^{-1} at 25°C , respectively, these modulated by a water-temperature dependent Arrhenius rate term. Because the concentration of dissolved CO_2 (referred to as $\text{CO}_{2(\text{aq})}$) in river water is derived not only from in-stream decomposition of DOC, but also from $\text{CO}_{2(\text{aq})}$ inputs from the decomposition of litter, SOC and DOC both in upland soils and in inundated soils, the model also represents the lateral transport of $\text{CO}_{2(\text{aq})}$ from soils through the river network. Note that autochthonous primary production and derivative carbon transformations are ignored here, as they are considered relatively minor contributors in the Arctic lateral flux system (Cauwet and Sidorov, 1996; Sorokin and Sorokin, 1996).

2.10 Dissolved CO_2 export and river evasion (Fig. 1j)

Soil $\text{CO}_{2(\text{aq})}$ exports are simulated by first assuming a constant concentration of $\text{CO}_{2(\text{aq})}$ with surface runoff and drainage water fluxes, of 20 and 2 mgC L^{-1} , corresponding to a $p\text{CO}_2$ of 50000 $\mu\text{ atm}$ and 5000 $\mu\text{ atm}$ at 25°C in the soil column, respectively. These quantities are then scaled with total (root, microbial, litter) soil respiration by a scaling factor first employed in Lauerwald et al. (2018, *in review*). In the high latitudes soil respiration is dominantly controlled by microbial decomposition, and for the Lena basin initial model tests suggest that its proportional contribution to total respiration is roughly 90%, versus 10% from root respiration. Thus $\text{CO}_{2(\text{aq})}$ enters and circulates the rivers via the same routing scheme as that for DOC and river water. The lateral transfers of carbon are aggregated from the 30 minute time steps at which they are calculated, with a 48 timestep period, so that they occur within the model as a daily flux. The calculation of the river network $p\text{CO}_2$ can then be made from $\text{CO}_{2(\text{aq})}$ and its equilibrium with the atmosphere, which is a function of its solubility (K_{CO_2}) with respect to the temperature of the water surface T_{WATER} (Eq.2).

$$(2) \quad p\text{CO}_{2\text{POOL}} = \frac{[\text{CO}_{2(\text{aq})}]}{12.011 * K_{\text{CO}_2}}$$

Where the $p\text{CO}_2$ of a given (e.g. 'stream', 'fast', 'slow' and floodplain) water pool ($p\text{CO}_{2\text{POOL}}$) is given by $[\text{CO}_{2(\text{aq})}]$ the dissolved CO_2 concentration in that pool, and K_{CO_2} . Water temperature (T_{WATER} , $^\circ\text{C}$) isn't simulated by the model, but is derived here from the average daily surface temperature (T_{GROUND} , $^\circ\text{C}$) in the model (Eq. 3), a set up used by Lauerwald et al. (2017) and retained here. Note that while dissolved CO_2 enters from



the terrestrial reservoir from organic matter decomposition, it is also generated *in situ* within the river network as DOC is respired microbially.

With our water temperature estimate, both K_{CO_2} and the Schmidt number (Sc) from Wanninkhof (1992) can be calculated, allowing for simulation of actual gas exchange velocities from standard conditions. The Schmidt number links the gas transfer velocity of any soluble gas (in this case carbon dioxide) from the water surface to water temperature. For more on the Schmidt number see (Wanninkhof, 2014, 1992). The CO_2 that evades is then subtracted from the $[CO_2]$ stocks of each of the different hydrologic reservoirs –river, flood and stream.

$$(3) \quad T_{WATER} = 6.13^\circ C + (0.8 * T_{GROUND})$$

$$(4) \quad Sc = ((1911 - 118.11) * T_{WATER}) + (3.453 * T_{WATER}^2) - (0.0413 * T_{WATER}^3)$$

CO_2 evasion is therefore assumed to originate from the interplay of CO_2 solubility, relative gradient in partial pressures of CO_2 between air and water, and gas exchange kinetics. Evasion as a flux from river and floodplain water surfaces is calculated at a daily timestep, however in order to satisfy the sensitivity of the relative gradient of partial pressures of CO_2 in the water column and atmosphere to both CO_2 inputs and evasion, the pCO_2 of water is calculated at a more refined 6 minute timestep. The daily lateral flux of CO_2 inputs to the water column are thus equally broken up into 240 (6 min.) segments per day and distributed to the pCO_2 calculation. Other relevant carbon processing pathways, such as the photochemical breakdown of riverine OC, are not explicitly included here, despite the suggestion by some studies that the photochemical pathway dominate DOC processing in Arctic streams (e.g. Cory et al., 2014). Rather, these processes are bundled into the aggregate decomposition rates used in the model, which thus include both microbial and photochemical oxidation. This is largely because it is unclear how different factors contribute to breaking down DOC in a dynamic environment and also the extent to which our DOC decomposition and CO_2 calculations implicitly include both pathways –e.g. to what extent the equations and concepts used in their calculation confound bacterial with photochemical causation, since both microbial activity and incident UV light are a function of temperature and total incident light.

2.11 Soil layer processes:urbation (Fig. 1k), adsorption (Fig. 1l)

The soil carbon module is discretised into a 32-layer scheme totalling 38m depth, which it shares with the soil thermodynamics to calculate temperature through the entire column. An aboveground snow module (Wang et al., 2013) is discretised into 3 layers of differing thickness, heat conductance and density, which collectively act as a thermodynamically-insulating intermediary between soil and atmosphere (Fig. 2a). Inputs to the three soil carbon pools are resolved only for the top 2m of the soil, where litter and DOC are exchanged with SOC in decomposition and adsorption/desorption processes. Decomposition of SOC pools, calculated in each soil layer, is dependent on soil temperature, moisture and texture (Koven et al., 2009; Zhu et al., 2016), while vertical transfer of SOC is enabled by representation of cryoturbation (downward movement of matter due to repeated freeze-thaw) in permafrost regions, and bioturbation (by soil organisms) in non-permafrost regions in terms of a diffusive flux.



680 Cryoturbation, given a diffusive mixing rate (*Diff*) of $0.001 \text{ m}^2 \text{ yr}^{-1}$ (Koven et al., 2009), is
 681 possible to 3 m depth (diffusive rate declines linearly to zero from active layer bottom to
 682 3 m), and extends the soil column carbon concentration depth in permafrost regions
 683 from 2 m. Bioturbation is possible to 2 m depth, with a mixing rate of $0.0001 \text{ m}^2 \text{ yr}^{-1}$
 684 (Koven et al., 2013) declining to zero at 2 m (Eq. 5). In MICT-L, these vertical exchanges
 685 in the soil column are improved on. Now, we explicitly include the cryoturbation and
 686 bioturbation of both belowground litter and DOC. These were not possible in
 687 ORCHIDEE-MICT because, for the former, the belowground litter distribution was not
 688 explicitly discretised or vertically dynamic, and for the latter because DOC was not
 689 produced in prior versions. Diffusion is given by :

$$((5)) \quad \frac{\delta \text{DOC}_i(z)}{\delta t} = \text{IN}_{\text{DOC}_i}(z) - k_i(z) * \Phi * \text{DOC}_i(z) + \text{Diff} \frac{\delta \text{DOC}_i^2(z)}{\delta z^2}$$

691
 692 Where DOC_i is the DOC in pool *i* at depth *z*, (gC m^{-3}) IN_{DOC_i} the inflow of carbon to that
 693 pool ($\text{gCm}^{-3}\text{d}^{-1}$), k_i the decomposition rate of that pool (d^{-1}), Φ the temperature
 694 dependent rate modifier for DOC decomposition and *Diff* the diffusion coefficient ($\text{m}^2 \text{ yr}^{-1}$).
 695 The vertical diffusion of DOC in non-permafrost soils represented here (that is, the
 696 non-cryoturbated component) appears to be consistent with recent studies reporting an
 697 increased retention of DOC in the deepening active layer of organic soils (Zhang et al.,
 698 2017). This vertical translocation of organic carbon, whether in solid/liquid phase
 699 appears to be an important component of the high rates of SOC buildup observed at
 700 depth in deep permafrost soils.

701 702 2.11 Priming (Fig. 1m)

703
 704 MICT-L also incorporates a scheme for the ‘priming’ of organic matter decomposition, a
 705 process in which the relative stability of SOC is impacted by the intrusion of or contact
 706 with SOC of greater reactivity, resulting in enhanced rates of decomposition. This was
 707 first introduced by Guenet et al. (2016) and updated in Guenet et al. (2018). This
 708 process has shown itself to be of potentially large significance for SOC stocks and their
 709 respiration in high latitude regions, in empirical in situ and soil incubation studies (De
 710 Baets et al., 2016; Walz et al., 2017; Wild et al., 2014, 2016; Zhang et al., 2017), as well as
 711 modelling exercises (Guenet et al., 2018). Here, priming of a given soil pool is
 712 represented through the decomposition of soil carbon (dSOC/dt) by the following
 713 equation :

$$(6) \quad \frac{\text{dSOC}}{\text{dt}} = \text{IN}_{\text{SOC}} - k * (1 - e^{-c*FOC}) * \text{SOC} * \Theta * \Phi * \gamma$$

715
 716 Where IN_{SOC} is the carbon input to that pool, *k* is the SOC decomposition rate, FOC is a
 717 stock of matter interacting with this SOC pool to produce priming, *c* is a parameter
 718 controlling this interaction, SOC is the SOC reservoir, and θ , Φ and γ the moisture,
 719 temperature and texture functions that modulate decomposition in the code. The
 720 variable FOC (‘fresh organic carbon’) is an umbrella term used for specifying all of the
 721 carbon pools which together constitute that carbon which is considered potential
 722 priming donor material –ie. more labile – to a given receptor carbon pool. Thus, for the
 723 slow soil carbon pool FOC incorporates the active soil carbon pool plus the above and
 724 below ground structural and metabolic litter pools, because these pools are donors to



the slow pool, and considered to accelerate its turnover through priming. Importantly, previous studies with priming in ORCHIDEE employed this scheme on a version which resolves neither the vertical discretisation of the soil column nor the explicit vertical diffusion processes presented here. This is potentially significant, since the vertical diffusion of relatively reactive matter may strongly impact (accelerate) the decomposition of low reactivity matter in the deeper non-frozen horizons of high latitude soils, while the explicit discretisation of the soil column is a significant improvement in terms of the accuracy of process-representation within the column itself.

Other carbon-relevant schemes included in MICT-L are: A prognostic fire routine (SPITFIRE), calibrated for the trunk version of ORCHIDEE (Yue et al., 2016) is available in our code but not activated in the simulations conducted here. As a result, we do not simulate the ~13% of Arctic riverine DOC attributed to biomass burning by Myers-Pigg et al. (2015), or the ~8% of DOC discharge to the Arctic Ocean from the same source (Stubbins et al., 2017). Likewise, a crop harvest module consistent with that in ORCHIDEE-MICT exists in MICT-L but remains deactivated for our simulations.

A module introduced in the last version of ORCHIDEE-MICT (Guimberteau et al., 2018), in which the soil thermal transfer and porosity and moisture are strongly affected by SOC concentration, is deactivated here, because it is inconsistent with the new DOC scheme. Specifically, while carbon is conserved in both MICT and MICT-L soil schemes, MICT-L introduces a new reservoir into which part of the total organic carbon in the soil –the DOC –must now go. This then lowers the SOC concentration being read by this thermix module, causing significant model artefact in soil thermodynamics and hydrology in early exploratory simulations. Ensuring compatibility of this routine with the DOC scheme will be a focal point of future developments in MICT-L. Other processes being developed for ORCHIDEE-MICT, including a high latitude peat formation (Qiu et al., 2018), methane production and microbial heat generating processes that are being optimised and calibrated, are further pending additions to this particular branch of the ORCHIDEE-MICT series.

3 Soil Carbon Spinup and Simulation Protocol

The soil carbon spinup component of ORCHIDEE, which is available to both its trunk and MICT branches, was omitted from this first version of MICT-L, owing to the code burden required for ensuring compability with the soil carbon scheme in MICT-L. However, because we are simulating high latitude permafrost regions, having a realistic soil carbon pool at the outset of the simulations is necessary if we are to untangle the dynamics of SOC and DOC with a changing environment. Because the soil carbon spinup in ORCHIDEE-MICT is normally run over more than 10,000 years (Guimberteau et al., 2108), and because running MICT-L for this simulation period in its normal, non-spinup simulation mode would impose an unreasonable burden on computing resources, here we directly force the soil carbon output from a MICT spinup directly into the restart file of a MICT-L simulation.

A 20,000 year spinup loop over 1961-1990 (these years chosen to mimic coarsely warmer mid-Holocene climate) -forced by GSWP-3 climatology, whose configuration derives directly from that used in Guimberteau et al. (2018), was thus used to replace



the three soil carbon pool values from a 1-year MICT-L simulation to set their initial values. A conversion of this soil carbon from volumetric to areal units was applied, owing to different read/write standards in ORCHILEAK versus ORCHIDEE-MICT. This artificially imposed, MICT-derived SOC stock would then have to be exposed to MICT-L code, whose large differences in soil carbon module architecture as compared to MICT, would drive a search for new equilibrium soil carbon stocks.

Due to the long residence times of the passive SOC pool, reaching full equilibrium for it requires a simulation length on the order of 20,000y –again an overburden. As we are interested primarily in DOC in this study, which derives mostly from the Active and Slow SOC pools, the model was run until these two pools reached a quasi-steady state equilibria (Part 2 Supplement, Fig. S1). This was done by looping over the same 30 year cycle (1901-1930) of climate forcing data from GSWP-3 during the pre-industrial period (Table 1) and the first year (1901) of a prescribed vegetation map (ESA CCI Land Cover Map, Bontemps et al., (2013)) –to ensure equilibrium of DOC, dissolved CO₂ and Active and Slow SOC pools is driven not just by a single set of environmental factors in one year –for a total of 400 years. The parameter configuration adhered as close as possible to that used in the original ORCHIDEE-MICT spinup simulations, to avoid excessive equilibrium drift from the original SOC state (Fig. 3).

4 Conclusion

This first part of a two-part study has described a new branch of the high latitude version of ORCHIDEE-MICT land surface model, in which the production, transport and transformation of DOC and dissolved CO₂ in soils and along the inland water network of explicitly-represented northern permafrost regions has been implemented for the first time. Novel processes with respect to ORCHIDEE-MICT include the discretisation of litter inputs to the soil column, the production of DOC and CO_{2(aq)} from organic matter and decomposition, respectively, transport of DOC into the river routing network and its potential mineralisation to CO_{2(aq)} in the water column, as well as subsequent evasion from the water surface to the atmosphere. In addition, an improved floodplains representation has been implemented which allows for the hydrologic cycling of DOC and CO₂ in these inundated areas. In addition to descriptions of these processes, this paper outlines the protocols and configuration adopted for simulations using this new model that will be used for its evaluation over the Lena river basin in the second part of this study.

Code and data availability

The source code for ORCHIDEE MICT-LEAK revision 5459 is available via http://forge.ipsl.jussieu.fr/orchidee/wiki/GroupActivities/CodeAvailabilityPublication/ORCHIDEE_gmd-2018-MICT-LEAK_r5459

Primary data and scripts used in the analysis and other supplementary information that may be useful in reproducing the author's work can be obtained by contacting the corresponding author.

This software is governed by the CeCILL license under French law and abiding by the rules of distribution of free software. You can use, modify and/or redistribute the



software under the terms of the CeCILL license as circulated by CEA, CNRS and INRIA at the following URL: <http://www.cecill.info>.

Authors' contribution

SB coded this model version, conducted the simulations and wrote the main body of the paper. RL gave consistent input to the coding process and made numerous code improvements and bug fixes. BG advised on the inclusion of priming processes in the model and advised on the study design and model configuration; DZ gave input on the modelled soil carbon processes and model configuration. MG, AT and AD contributed to improvements in hydrological representation and floodplain forcing data. PC oversaw all developments leading to the publication of this study. All authors contributed to suggestions regarding the final content of the study.

Competing interests

The authors declare no competing financial interests.

Acknowledgements

Simon Bowring acknowledges funding from the European Union's Horizon 2020 research and innovation program under the Marie Skłodowska-Curie grant agreement No. 643052, 'C-CASCADES' program. Simon Bowring received a PhD grant. Matthieu Guimberteau acknowledges funding from the European Research Council Synergy grant ERC-2013-SyG-610028 IMBALANCE-P. Ronny Lauerwald acknowledges funding from the European Union's Horizon 2020 research and innovation program under grant agreement no.703813 for the Marie Skłodowska-Curie European Individual Fellowship "C-Leak".

References:

- Aitkenhead-Peterson, J. A., McDowell, W. H. and Neff, J. C.: Sources, Production, and Regulation of Allochthonous Dissolved Organic Matter Inputs to Surface Waters, in *Aquatic Ecosystems*, 2003.
- De Baets, S., Van de Weg, M. J., Lewis, R., Steinberg, N., Meersmans, J., Quine, T. A., Shaver, G. R. and Hartley, I. P.: Investigating the controls on soil organic matter decomposition in tussock tundra soil and permafrost after fire, *Soil Biol. Biochem.*, doi:10.1016/j.soilbio.2016.04.020, 2016.
- Bardy, M., Derenne, S., Allard, T., Benedetti, M. F. and Fritsch, E.: Podzolisation and exportation of organic matter in black waters of the Rio Negro (upper Amazon basin, Brazil), *Biogeochemistry*, doi:10.1007/s10533-010-9564-9, 2011.
- Bauch, D., Hölemann, J. A., Nikulina, A., Wegner, C., Janout, M. A., Timokhov, L. A. and Kassens, H.: Correlation of river water and local sea-ice melting on the Laptev Sea shelf (Siberian Arctic), *J. Geophys. Res. Ocean.*, doi:10.1002/jgrc.20076, 2013.
- Berezovskaya, S., Yang, D. and Hinzman, L.: Long-term annual water balance analysis of the Lena River, *Glob. Planet. Change*, doi:10.1016/j.gloplacha.2004.12.006, 2005.
- Bergkvist, B. O. and Folkeson, L.: Soil acidification and element fluxes of a *Fagus sylvatica* forest as influenced by simulated nitrogen deposition, *Water, Air, Soil Pollut.*, doi:10.1007/BF00482753, 1992.
- Bontemps, S., Defourny, P., Radoux, J., Van Bogaert, E., Lamarche, C., Achard, F., Mayaux, P., Boettcher, M., Brockmann, C., Kirches, G., Zülke, M., Kalogirou, V., Seifert, F. and Arino, O.: Consistent global land cover maps for climate modelling communities: current



- 871 achievements of the ESA' and cover CCI, in ESA Living Planet Symposium 2013., 2013.
872 Camino-Serrano, M., Gielen, B., Luyssaert, S., Ciais, P., Vicca, S., Guenet, B., Vos, B. De,
873 Cools, N., Ahrens, B., Altaf Arain, M., Borken, W., Clarke, N., Clarkson, B., Cummins, T.,
874 Don, A., Pannatier, E. G., Laudon, H., Moore, T., Nieminen, T. M., Nilsson, M. B., Peichl, M.,
875 Schwendenmann, L., Siemens, J. and Janssens, I.: Linking variability in soil solution
876 dissolved organic carbon to climate, soil type, and vegetation type, *Global Biogeochem.*
877 *Cycles*, doi:10.1002/2013GB004726, 2014.
878 Camino-Serrano, M., Guenet, B., Luyssaert, S., Ciais, P., Bastrikov, V., De Vos, B., Gielen, B.,
879 Gleixner, G., Jornet-Puig, A., Kaiser, K., Kothawala, D., Lauerwald, R., Peñuelas, J.,
880 Schrumpf, M., Vicca, S., Vuichard, N., Walmsley, D. and Janssens, I. A.: ORCHIDEE-SOM:
881 Modeling soil organic carbon (SOC) and dissolved organic carbon (DOC) dynamics along
882 vertical soil profiles in Europe, *Geosci. Model Dev.*, doi:10.5194/gmd-11-937-2018,
883 2018.
884 Cauwet, G. and Sidorov, I.: The biogeochemistry of Lena River: Organic carbon and
885 nutrients distribution, in *Marine Chemistry*., 1996.
886 Clarke, N., Wu, Y. and Strand, L. T.: Dissolved organic carbon concentrations in four
887 Norway spruce stands of different ages, *Plant Soil*, doi:10.1007/s11104-007-9384-4,
888 2007.
889 Cory, R. M., Ward, C. P., Crump, B. C. and Kling, G. W.: Sunlight controls water column
890 processing of carbon in arctic fresh waters, *Science* (80-.),
891 doi:10.1126/science.1253119, 2014.
892 D'Orgeval, T., Polcher, J. and De Rosnay, P.: Sensitivity of the West African hydrological
893 cycle in ORCHIDEE to infiltration processes, *Hydrol. Earth Syst. Sci.*, doi:10.5194/hess-
894 12-1387-2008, 2008.
895 DeLuca, T. H. and Boisvenue, C.: Boreal forest soil carbon: Distribution, function and
896 modelling, *Forestry*, doi:10.1093/forestry/cps003, 2012.
897 Denfeld, B., Frey, K. and Sobczak, W.: Summer CO₂ evasion from streams and rivers in
898 the Kolyma River basin, north-east Siberia, *Polar ...*, doi:10.3402/polar.v32i0.19704,
899 2013.
900 Dery, S. J., Stadnyk, T. A., MacDonald, M. K. and Gaudi-Sharma, B.: Recent trends and
901 variability in river discharge across northern Canada, *Hydrol. Earth Syst. Sci.*,
902 doi:10.5194/hess-20-4801-2016, 2016.
903 Drake, T. W., Wickland, K. P., Spencer, R. G. M., McKnight, D. M. and Striegl, R. G.: Ancient
904 low-molecular-weight organic acids in permafrost fuel rapid carbon dioxide production
905 upon thaw, *Proc. Natl. Acad. Sci.*, doi:10.1073/pnas.1511705112, 2015.
906 Ducharne, A., Golaz, C., Leblois, E., Laval, K., Polcher, J., Ledoux, E. and De Marsily, G.:
907 Development of a high resolution runoff routing model, calibration and application to
908 assess runoff from the LMD GCM, *J. Hydrol.*, doi:10.1016/S0022-1694(03)00230-0,
909 2003.
910 Findlay, H. S., Gibson, G., Kędra, M., Morata, N., Orchowska, M., Pavlov, A. K., Reigstad, M.,
911 Silyakova, A., Tremblay, J.-É., Walczowski, W., Weydmann, A. and Logvinova, C.:
912 Responses in Arctic marine carbon cycle processes: conceptual scenarios and
913 implications for ecosystem function, *Polar Res.*, doi:10.3402/polar.v34.24252, 2015.
914 Fluet-Chouinard, E., Lehner, B., Rebelo, L. M., Papa, F. and Hamilton, S. K.: Development
915 of a global inundation map at high spatial resolution from topographic downscaling of
916 coarse-scale remote sensing data, *Remote Sens. Environ.*, doi:10.1016/j.rse.2014.10.015,
917 2015.
918 Fröberg, M., Berggren, D., Bergkvist, B., Bryant, C. and Mulder, J.: Concentration and
919 fluxes of dissolved organic carbon (DOC) in three Norway spruce stands along a climatic



- 920 gradient in Sweden, Biogeochemistry, doi:10.1007/s10533-004-0564-5, 2006.
- 921 Gouttevin, I., Menegoz, M., Dominé, F., Krinner, G., Koven, C., Ciais, P., Tarnocai, C. and
- 922 Boike, J.: How the insulating properties of snow affect soil carbon distribution in the
- 923 continental pan-Arctic area, J. Geophys. Res. Biogeosciences,
- 924 doi:10.1029/2011JG001916, 2012.
- 925 Graham, D. E., Wallenstein, M. D., Vishnivetskaya, T. A., Waldrop, M. P., Phelps, T. J.,
- 926 Pfiffner, S. M., Onstott, T. C., Whyte, L. G., Rivkina, E. M., Gilichinsky, D. A., Elias, D. A.,
- 927 MacKelpiang, R., Verberkmoes, N. C., Hettich, R. L., Wagner, D., Wulfschleger, S. D. and
- 928 Jansson, J. K.: Microbes in thawing permafrost: The unknown variable in the climate
- 929 change equation, ISME J., doi:10.1038/ismej.2011.163, 2012.
- 930 Guenet, B., Moyano, F. E., Peylin, P., Ciais, P. and Janssens, I. A.: Towards a representation
- 931 of priming on soil carbon decomposition in the global land biosphere model ORCHIDEE
- 932 (version 1.9.5.2), Geosci. Model Dev., doi:10.5194/gmd-9-841-2016, 2016.
- 933 Guenet, B., Camino-Serrano, M., Ciais, P., Tifafi, M., Maignan, F., Soong, J. L. and Janssens,
- 934 I. A.: Impact of priming on global soil carbon stocks, Glob. Chang. Biol.,
- 935 doi:10.1111/gcb.14069, 2018.
- 936 Guimberteau, M., Drapeau, G., Ronchail, J., Sultan, B., Polcher, J., Martinez, J. M., Prigent,
- 937 C., Guyot, J. L., Cochonneau, G., Espinoza, J. C., Filizola, N., Fraizy, P., Lavado, W., De
- 938 Oliveira, E., Pombosa, R., Noriega, L. and Vauchel, P.: Discharge simulation in the sub-
- 939 basins of the Amazon using ORCHIDEE forced by new datasets, Hydrol. Earth Syst. Sci.,
- 940 doi:10.5194/hess-16-911-2012, 2012.
- 941 Guimberteau, M., Zhu, D., Maignan, F., Huang, Y., Yue, C., Dantec-N d lec, S., Ottl, C., Jornet-
- 942 Puig, A., Bastos, A., Laurent, P., Goll, D., Bowring, S., Chang, J., Guenet, B., Tifafi, M., Peng,
- 943 S., Krinner, G., Ducharne, A. s., Wang, F., Wang, T., Wang, X., Wang, Y., Yin, Z., Lauerwald,
- 944 R., Joetzjer, E., Qiu, C., Kim, H. and Ciais, P.: ORCHIDEE-MICT (v8.4.1), a land surface
- 945 model for the high latitudes: model description and validation, Geosci. Model Dev.,
- 946 doi:10.5194/gmd-11-121-2018, 2018.
- 947 Heim, B., Abramova, E., Doerffer, R., Günther, F., Hölemann, J., Kraberg, A., Lantuit, H.,
- 948 Loginova, A., Martynov, F., Overduin, P. P. and Wegner, C.: Ocean colour remote sensing
- 949 in the southern laptev sea: Evaluation and applications, Biogeosciences, doi:10.5194/bg-
- 950 11-4191-2014, 2014.
- 951 Hollesen, J., Matthiesen, H., Møller, A. B. and Elberling, B.: Permafrost thawing in organic
- 952 Arctic soils accelerated by ground heat production, Nat. Clim. Chang.,
- 953 doi:10.1038/nclimate2590, 2015.
- 954 Holmes, R. M., McClelland, J. W., Peterson, B. J., Tank, S. E., Bulygina, E., Eglinton, T. I.,
- 955 Gordeev, V. V., Gurtovaya, T. Y., Raymond, P. A., Repeta, D. J., Staples, R., Striegl, R. G.,
- 956 Zhulidov, A. V. and Zimov, S. A.: Seasonal and Annual Fluxes of Nutrients and Organic
- 957 Matter from Large Rivers to the Arctic Ocean and Surrounding Seas, Estuaries and
- 958 Coasts, doi:10.1007/s12237-011-9386-6, 2012.
- 959 Hugelius, G., Bockheim, J. G., Camill, P., Elberling, B., Grosse, G., Harden, J. W., Johnson, K.,
- 960 Jorgenson, T., Koven, C. D., Kuhry, P., Michaelson, G., Mishra, U., Palmtag, J., Ping, C.-L.,
- 961 O'Donnell, J., Schirrmeister, L., Schuur, E. A. G., Sheng, Y., Smith, L. C., Strauss, J. and Yu, Z.: A new data set for estimating organic carbon storage to 3m depth in soils of the
- 962 northern circumpolar permafrost region, EARTH Syst. Sci. DATA, doi:10.5194/essd-5-
- 963 393-2013, 2013.
- 964 Hugelius, G., Strauss, J., Zubrzycki, S., Harden, J. W., Schuur, E. A. G., Ping, C. L.,
- 965 Schirrmeister, L., Grosse, G., Michaelson, G. J., Koven, C. D., O'Donnell, J. A., Elberling, B.,
- 966 Mishra, U., Camill, P., Yu, Z., Palmtag, J. and Kuhry, P.: Estimated stocks of circumpolar
- 967 permafrost carbon with quantified uncertainty ranges and identified data gaps,
- 968



- 969 Biogeosciences, doi:10.5194/bg-11-6573-2014, 2014.
- 970 Jakobsson, M.: Hypsometry and volume of the Arctic Ocean and its constituent seas,
- 971 Geochemistry, Geophys. Geosystems, doi:10.1029/2001GC000302, 2002.
- 972 Janout, M., Håflemann, J., Juhls, B., Krumpen, T., Rabe, B., Bauch, D., Wegner, C., Kassens,
- 973 H. and Timokhov, L.: Episodic warming of near-bottom waters under the Arctic sea ice
- 974 on the central Laptev Sea shelf, Geophys. Res. Lett., doi:10.1002/2015GL066565, 2016.
- 975 Jasechko, S., Kirchner, J. W., Welker, J. M. and McDonnell, J. J.: Substantial proportion of
- 976 global streamflow less than three months old, Nat. Geosci., doi:10.1038/ngeo2636, 2016.
- 977 Kicklighter, D. W., Hayes, D. J., McClelland, J. W., Peterson, B. J., McGuire, A. D. and Melillo,
- 978 J. M.: Insights and issues with simulating terrestrial DOC loading of Arctic river
- 979 networks, Ecol. Appl., doi:10.1890/11-1050.1, 2013.
- 980 Koven, C., Friedlingstein, P., Ciais, P., Khvorostyanov, D., Krinner, G. and Tarnocai, C.: On
- 981 the formation of high-latitude soil carbon stocks: Effects of cryoturbation and insulation
- 982 by organic matter in a land surface model, Geophys. Res. Lett.,
- 983 doi:10.1029/2009GL040150, 2009.
- 984 Koven, C. D., Riley, W. J., Subin, Z. M., Tang, J. Y., Torn, M. S., Collins, W. D., Bonan, G. B.,
- 985 Lawrence, D. M. and Swenson, S. C.: The effect of vertically resolved soil biogeochemistry
- 986 and alternate soil C and N models on C dynamics of CLM4, Biogeosciences,
- 987 doi:10.5194/bg-10-7109-2013, 2013.
- 988 Krinner, G., Viovy, N., de Noblet-Ducoudré, N., Ogée, J., Polcher, J., Friedlingstein, P., Ciais,
- 989 P., Sitch, S. and Prentice, I. C.: A dynamic global vegetation model for studies of the
- 990 coupled atmosphere-biosphere system, Global Biogeochem. Cycles,
- 991 doi:10.1029/2003GB002199, 2005.
- 992 Kunkel, K. E., Robinson, D. A., Champion, S., Yin, X., Estilow, T. and Frankson, R. M.: Trends and Extremes in Northern Hemisphere Snow Characteristics, Curr. Clim. Chang.
- 993 Reports, doi:10.1007/s40641-016-0036-8, 2016.
- 994 Kutscher, L., Mörtz, C. M., Porcelli, D., Hirst, C., Maximov, T. C., Petrov, R. E. and
- 995 Andersson, P. S.: Spatial variation in concentration and sources of organic carbon in the
- 996 Lena River, Siberia, J. Geophys. Res. Biogeosciences, doi:10.1002/2017JG003858, 2017.
- 997 Lammers, R. B., Pundsack, J. W. and Shiklomanov, A. I.: Variability in river temperature,
- 998 discharge, and energy flux from the Russian pan-Arctic landmass, J. Geophys. Res.
- 1000 Biogeosciences, doi:10.1029/2006JG000370, 2007.
- 1001 Lauerwald, R., Regnier, P., Camino-Serrano, M., Guenet, B., Guimberteau, M., Ducharne,
- 1002 A., Polcher, J. and Ciais, P.: ORCHILEAK (revision 3875): A new model branch to simulate
- 1003 carbon transfers along the terrestrial-aquatic continuum of the Amazon basin, Geosci.
- 1004 Model Dev., doi:10.5194/gmd-10-3821-2017, 2017.
- 1005 Lindroos, A. J., Derome, J., Derome, K. and Smolander, A.: The effect of scots pine, norway
- 1006 spruce and silver birch on the chemical composition of stand throughfall and upper soil
- 1007 percolation water in northern Finland, Boreal Environ. Res., 2011.
- 1008 MacKelpirang, R., Waldrop, M. P., Deangelis, K. M., David, M. M., Chavarria, K. L.,
- 1009 Blazewicz, S. J., Rubin, E. M. and Jansson, J. K.: Metagenomic analysis of a permafrost
- 1010 microbial community reveals a rapid response to thaw, Nature,
- 1011 doi:10.1038/nature10576, 2011.
- 1012 Mann, P. J., Eglinton, T. I., McIntyre, C. P., Zimov, N., Davydova, A., Vonk, J. E., Holmes, R.
- 1013 M. and Spencer, R. G. M.: Utilization of ancient permafrost carbon in headwaters of Arctic
- 1014 fluvial networks, Nat. Commun., doi:10.1038/ncomms8856, 2015.
- 1015 Manning, R.: On the Flow of Water in Open Channels and Pipes, Trans. Inst. Civ. Eng. Irel.,
- 1016 doi:10.1021/bi2010619, 1891.
- 1017 Manzoni, S., Taylor, P., Richter, A., Porporato, A. and Ågren, G. I.: Environmental and



- 1018 stoichiometric controls on microbial carbon-use efficiency in soils, *New Phytol.*,
1019 doi:10.1111/j.1469-8137.2012.04225.x, 2012.
- 1020 McClelland, J. W., Holmes, R. M., Dunton, K. H. and Macdonald, R. W.: The Arctic Ocean
1021 Estuary, *Estuaries and Coasts*, doi:10.1007/s12237-010-9357-3, 2012.
- 1022 McClelland, J. W., Holmes, R. M., Peterson, B. J., Raymond, P. A., Striegl, R. G., Zhulidov, A.
1023 V., Zimov, S. A., Zimov, N., Tank, S. E., Spencer, R. G. M., Staples, R., Gurtovaya, T. Y. and
1024 Griffin, C. G.: Particulate organic carbon and nitrogen export from major Arctic rivers,
1025 *Global Biogeochem. Cycles*, doi:10.1002/2015GB005351, 2016.
- 1026 McGuire, A. D., Anderson, L. G., Christensen, T. R., Dallimore, S., Guo, L., Hayes, D. J.,
1027 Heimann, M., Lorenson, T. D., Macdonald, R. W. and Roulet, N.: Sensitivity of the carbon
1028 cycle in the Arctic to climate change, *Ecol. Monogr.*, doi:10.1890/08-2025.1, 2009.
- 1029 Messenger, M. L., Lehner, B., Grill, G., Nedeva, I. and Schmitt, O.: Estimating the volume and
1030 age of water stored in global lakes using a geo-statistical approach, *Nat. Commun.*,
1031 doi:10.1038/ncomms13603, 2016.
- 1032 Mudryk, L. R., Derksen, C., Kushner, P. J. and Brown, R.: Characterization of Northern
1033 Hemisphere snow water equivalent datasets, 1981-2010, *J. Clim.*, doi:10.1175/JCLI-D-
1034 15-0229.1, 2015.
- 1035 Myers-Pigg, A. N., Louchouart, P., Amon, R. M. W., Prokushkin, A., Pierce, K. and Rubtsov,
1036 A.: Labile pyrogenic dissolved organic carbon in major Siberian Arctic rivers:
1037 Implications for wildfire-stream metabolic linkages, *Geophys. Res. Lett.*,
1038 doi:10.1002/2014GL062762, 2015.
- 1039 Nachtergaele, F. et al.: The harmonized world soil database, FAO, ISRIC, ISSCAS, JRC,
1040 doi:10.1017/9781107300000, 2010.
- 1041 Ngo-Duc, T., Laval, K., Ramillien, G., Polcher, J. and Cazenave, A.: Validation of the land
1042 water storage simulated by Organising Carbon and Hydrology in Dynamic Ecosystems
1043 (ORCHIDEE) with Gravity Recovery and Climate Experiment (GRACE) data, *Water*
1044 *Resour. Res.*, doi:10.1029/2006WR004941, 2007.
- 1045 O'Donnell, J. A., Aiken, G. R., Swanson, D. K., Panda, S., Butler, K. D. and Baltensperger, A.
1046 P.: Dissolved organic matter composition of Arctic rivers: Linking permafrost and parent
1047 material to riverine carbon, *Global Biogeochem. Cycles*, doi:10.1002/2016GB005482,
1048 2016.
- 1049 Oki, T., Nishimura, T. and Dirmeyer, P. A.: Assessment of annual runoff from land surface
1050 models using Total Runoff Integrating Pathways (TRIP), *J. Meteorol. Soc. Japan*, 1999.
- 1051 Pekel, J.-F., Cottam, A., Gorelick, N. and Belward, A. S.: Global Surface Water - Data Users
1052 Guide (JRC) High-resolution mapping of global surface water and its long-term changes,
1053 *Nature*, doi:10.1038/nature20584, 2016.
- 1054 Peterson, B. J., Holmes, R. M., McClelland, J. W., Vörösmarty, C. J., Lammers, R. B.,
1055 Shiklomanov, A. I., Shiklomanov, I. A. and Rahmstorf, S.: Increasing river discharge to the
1056 Arctic Ocean, *Science* (80-.), doi:10.1126/science.1077445, 2002.
- 1057 Ponomarev, E. I., Kharuk, V. I. and Ranson, K. J.: Wildfires dynamics in Siberian larch
1058 forests, *Forests*, doi:10.3390/f7060125, 2016.
- 1059 Prigent, C., Papa, F., Aires, F., Rossow, W. B. and Matthews, E.: Global inundation
1060 dynamics inferred from multiple satellite observations, 1993-2000, *J. Geophys. Res.*
1061 *Atmos.*, doi:10.1029/2006JD007847, 2007.
- 1062 Qiu, C., Zhu, D., Ciais, P., Guenet, B., Krinner, G., Peng, S., Aurela, M., Bernhofer, C.,
1063 Brümmer, C., Bret-Harte, S., Chu, H., Chen, J., Desai, A. R., Dušek, J., Euskirchen, E. S.,
1064 Fortuniak, K., Flanagan, L. B., Friborg, T., Grygoruk, M., Gogo, S., Grünwald, T., Hansen, B.
1065 U., Holl, D., Humphreys, E., Hurkuck, M., Kiely, G., Klatt, J., Kutzbach, L., Langeron, C.,
1066 Laggoun-Défarge, F., Lund, M., Lafleur, P. M., Li, X., Mammarella, I., Merbold, L., Nilsson,



- 1067 M. B., Olejnik, J., Ottosson-Löfvenius, M., Oechel, W., Parmentier, F. J. W., Peichl, M., Pirk,
1068 N., Peltola, O., Pawlak, W., Rasse, D., Rinne, J., Shaver, G., Peter Schmid, H., Sottocornola,
1069 M., Steinbrecher, R., Sachs, T., Urbaniak, M., Zona, D. and Ziemblinska, K.: ORCHIDEE-
1070 PEAT (revision 4596), a model for northern peatland CO₂, water, and energy fluxes on
1071 daily to annual scales, *Geosci. Model Dev.*, doi:10.5194/gmd-11-497-2018, 2018.
- 1072 Raymond, P. A., McClelland, J. W., Holmes, R. M., Zhulidov, A. V., Mull, K., Peterson, B. J.,
1073 Striegl, R. G., Aiken, G. R. and Gurtovaya, T. Y.: Flux and age of dissolved organic carbon
1074 exported to the Arctic Ocean: A carbon isotopic study of the five largest arctic rivers,
1075 *Global Biogeochem. Cycles*, doi:10.1029/2007GB002934, 2007.
- 1076 Rhein, M., Rintoul, S., Aoki, S., Campos, E., Chambers, D., Feely, R. A., Gulev, S., Johnson, G.,
1077 Josey, S., Kostianoy, A., Mauritzen, C., Roemmich, D., Talley, L., Wang, F. and IPCC:
1078 Observations: Ocean. In: *Climate Change 2013: The Physical Science Basis. Contribution*
1079 *of Working Group I to the Fifth Assessment Report of the Intergovernmental Panel on*
1080 *Climate Change.*, 2013.
- 1081 Rosenqvist, L., Hansen, K., Vesterdal, L. and van der Salm, C.: Water balance in
1082 afforestation chronosequences of common oak and Norway spruce on former arable
1083 land in Denmark and southern Sweden, *Agric. For. Meteorol.*,
1084 doi:10.1016/j.agrformet.2009.10.004, 2010.
- 1085 Schuur, E. A. G., Vogel, J. G., Crummer, K. G., Lee, H., Sickman, J. O. and Osterkamp, T. E.:
1086 The effect of permafrost thaw on old carbon release and net carbon exchange from
1087 tundra, *Nature*, doi:10.1038/nature08031, 2009.
- 1088 Schuur, E. A. G., McGuire, A. D., Schädel, C., Grosse, G., Harden, J. W., Hayes, D. J., Hugelius,
1089 G., Koven, C. D., Kuhry, P., Lawrence, D. M., Natali, S. M., Olefeldt, D., Romanovsky, V. E.,
1090 Schaefer, K., Turetsky, M. R., Treat, C. C. and Vonk, J. E.: Climate change and the
1091 permafrost carbon feedback, *Nature*, doi:10.1038/nature14338, 2015.
- 1092 Selvam, B. P., Lapierre, J. F., Guillemette, F., Voigt, C., Lamprecht, R. E., Biasi, C.,
1093 Christensen, T. R., Martikainen, P. J. and Berggren, M.: Degradation potentials of
1094 dissolved organic carbon (DOC) from thawed permafrost peat, *Sci. Rep.*,
1095 doi:10.1038/srep45811, 2017.
- 1096 Serreze, M. C. and Barry, R. G.: Processes and impacts of Arctic amplification: A research
1097 synthesis, *Glob. Planet. Change*, doi:10.1016/j.gloplacha.2011.03.004, 2011.
- 1098 Shakhova, N., Semiletov, I., Sergienko, V., Lobkovsky, L., Yusupov, V., Salyuk, A.,
1099 Salomatin, A., Chernykh, D., Kosmach, D., Panteleev, G., Nicolsky, D., Samarkin, V., Joye, S.,
1100 Charkin, A., Dudarev, O., Meluzov, A. and Gustafsson, O.: The East Siberian Arctic Shelf:
1101 Towards further assessment of permafrost-related methane fluxes and role of sea ice,
1102 *Philos. Trans. R. Soc. A Math. Phys. Eng. Sci.*, doi:10.1098/rsta.2014.0451, 2015.
- 1103 Smith, L. C. and Pavelsky, T. M.: Estimation of river discharge, propagation speed, and
1104 hydraulic geometry from space: Lena River, Siberia, *Water Resour. Res.*,
1105 doi:10.1029/2007WR006133, 2008.
- 1106 Sorokin, Y. I. and Sorokin, P. Y.: Plankton and primary production in the Lena River
1107 Estuary and in the south-eastern Laptev sea, *Estuar. Coast. Shelf Sci.*,
1108 doi:10.1006/ecss.1996.0078, 1996.
- 1109 Spencer, R. G. M., Mann, P. J., Dittmar, T., Eglinton, T. I., McIntyre, C., Holmes, R. M., Zimov,
1110 N. and Stubbins, A.: Detecting the signature of permafrost thaw in Arctic rivers, *Geophys.*
1111 *Res. Lett.*, doi:10.1002/2015GL063498, 2015.
- 1112 Starr, M., Lindroos, A. J., Ukonmaanaho, L., Tarvainen, T. and Tanskanen, H.: Weathering
1113 release of heavy metals from soil in comparison to deposition, litterfall and leaching
1114 fluxes in a remote, boreal coniferous forest, *Appl. Geochemistry*, doi:10.1016/S0883-
1115 2927(02)00157-9, 2003.



- 1116 Steele, M. and Ermold, W.: Loitering of the retreating sea ice edge in the Arctic Seas, J.
- 1117 Geophys. Res. Ocean., doi:10.1002/2015JC011182, 2015.
- 1118 Stroeve, J. C., Markus, T., Boisvert, L., Miller, J. and Barrett, A.: Changes in Arctic melt
- 1119 season and implications for sea ice loss, Geophys. Res. Lett.,
- 1120 doi:10.1002/2013GL058951, 2014.
- 1121 Stubbins, A., Mann, P. J., Powers, L., Bittar, T. B., Dittmar, T., McIntyre, C. P., Eglinton, T. I.,
- 1122 Zimov, N. and Spencer, R. G. M.: Low photolability of yedoma permafrost dissolved
- 1123 organic carbon, J. Geophys. Res. Biogeosciences, doi:10.1002/2016JG003688, 2017.
- 1124 Tank, S. E., Fellman, J. B., Hood, E. and Kritzbeg, E. S.: Beyond respiration: Controls on
- 1125 lateral carbon fluxes across the terrestrial-aquatic interface, Limnol. Oceanogr. Lett.,
- 1126 doi:10.1002/lol2.10065, 2018.
- 1127 Tarnocai, C., Canadell, J. G., Schuur, E. A. G., Kuhry, P., Mazhitova, G. and Zimov, S.: Soil
- 1128 organic carbon pools in the northern circumpolar permafrost retion, Global Biogeochem.
- 1129 Cycles, doi:10.1029/2008gb003327, 2009.
- 1130 Tootchi, A., Jost, A. and Ducharne, A.: Multi-source global wetland maps combining
- 1131 surface water imagery and groundwater constraints, Earth Syst. Sci. Data,
- 1132 doi:10.5194/essd-11-189-2019, 2019.
- 1133 Venkiteswaran, J. J., Schiff, S. L. and Wallin, M. B.: Large carbon dioxide fluxes from
- 1134 headwater boreal and sub-boreal streams, PLoS One,
- 1135 doi:10.1371/journal.pone.0101756, 2014.
- 1136 Vitousek, P. M. and Hobbie, S.: Heterotrophic nitrogen fixation in decomposing litter:
- 1137 Patterns and regulation, Ecology, doi:10.1890/0012-
- 1138 9658(2000)081[2366:HNFDL]2.0.CO;2, 2000.
- 1139 Vitousek, P. M. and Sanford, R. L.: Nutrient Cycling in Moist Tropical Forest, Ecology,
- 1140 doi:10.1146/annurev.es.17.110186.001033, 1986.
- 1141 Van Vliet, M. T. H., Yearsley, J. R., Franssen, W. H. P., Ludwig, F., Haddeland, I.,
- 1142 Lettenmaier, D. P. and Kabat, P.: Coupled daily streamflow and water temperature
- 1143 modelling in large river basins, Hydrol. Earth Syst. Sci., doi:10.5194/hess-16-4303-2012,
- 1144 2012.
- 1145 Van Vliet, M. T. H., Franssen, W. H. P., Yearsley, J. R., Ludwig, F., Haddeland, I.,
- 1146 Lettenmaier, D. P. and Kabat, P.: Global river discharge and water temperature under
- 1147 climate change, Glob. Environ. Chang., doi:10.1016/j.gloenvcha.2012.11.002, 2013.
- 1148 Vonk, J. E., Mann, P. J., Davydov, S., Davydova, A., Spencer, R. G. M., Schade, J., Sobczak, W.
- 1149 V., Zimov, N., Zimov, S., Bulygina, E., Eglinton, T. I. and Holmes, R. M.: High biolability of
- 1150 ancient permafrost carbon upon thaw, Geophys. Res. Lett., doi:10.1002/grl.50348, 2013.
- 1151 Vonk, J. E., Tank, S. E., Mann, P. J., Spencer, R. G. M., Treat, C. C., Striegl, R. G., Abbott, B. W.
- 1152 and Wickland, K. P.: Biodegradability of dissolved organic carbon in permafrost soils and
- 1153 aquatic systems: A meta-analysis, Biogeosciences, doi:10.5194/bg-12-6915-2015,
- 1154 2015a.
- 1155 Vonk, J. E., Tank, S. E., Bowden, W. B., Laurion, I., Vincent, W. F., Alekseychik, P., Amyot,
- 1156 M., Billet, M. F., Canário, J., Cory, R. M., Deshpande, B. N., Helbig, M., Jammet, M., Karlsson,
- 1157 J., Larouche, J., MacMillan, G., Rautio, M., Walter Anthony, K. M. and Wickland, K. P.:
- 1158 Reviews and Syntheses: Effects of permafrost thaw on arctic aquatic ecosystems,
- 1159 Biogeosciences Discuss., doi:10.5194/bg-12-10719-2015, 2015b.
- 1160 Vorosmarty, C. J., Fekete, B. M., Meybeck, M. and Lammers, R. B.: Global system of rivers:
- 1161 Its role in organizing continental land mass and defining land-To-Ocean linkages, Global
- 1162 Biogeochem. Cycles, doi:10.1029/1999GB900092, 2000.
- 1163 Walz, J., Knoblauch, C., Böhme, L. and Pfeiffer, E. M.: Regulation of soil organic matter
- 1164 decomposition in permafrost-affected Siberian tundra soils - Impact of oxygen



- 1165 availability, freezing and thawing, temperature, and labile organic matter, *Soil Biol.*
- 1166 *Biochem.*, doi:10.1016/j.soilbio.2017.03.001, 2017.
- 1167 Wang, T., Ottlé, C., Boone, A., Ciais, P., Brun, E., Morin, S., Krinner, G., Piao, S. and Peng, S.:
- 1168 Evaluation of an improved intermediate complexity snow scheme in the ORCHIDEE land
- 1169 surface model, *J. Geophys. Res. Atmos.*, doi:10.1002/jgrd.50395, 2013.
- 1170 Wanninkhof, R.: Relationship between wind speed and gas exchange over the ocean
- 1171 revisited, *Limnol. Oceanogr. Methods*, doi:10.4319/lom.2014.12.351, 2014.
- 1172 Wanninkhof, R. H.: Relationship between wind speed and gas exchange, *J. Geophys. Res.*,
- 1173 doi:10.1029/92JC00188, 1992.
- 1174 Whitefield, J., Winsor, P., McClelland, J. and Menemenlis, D.: A new river discharge and
- 1175 river temperature climatology data set for the pan-Arctic region, *Ocean Model.*,
- 1176 doi:10.1016/j.ocemod.2014.12.012, 2015.
- 1177 Wickland, K. P., Waldrop, M. P., Aiken, G. R., Koch, J. C., Jorgenson, M. T. and Striegl, R. G.:
- 1178 Dissolved organic carbon and nitrogen release from boreal Holocene permafrost and
- 1179 seasonally frozen soils of Alaska, *Environ. Res. Lett.*, doi:10.1088/1748-9326/aac4ad,
- 1180 2018.
- 1181 Wild, B., Schnecker, J., Alves, R. J. E., Barsukov, P., Bárta, J., Čapek, P., Gentsch, N., Gittel, A.,
- 1182 Guggenberger, G., Lashchinskiy, N., Mikutta, R., Rusalimova, O., Šantrůčková, H.,
- 1183 Shibistova, O., Urich, T., Watzka, M., Zrazhevskaya, G. and Richter, A.: Input of easily
- 1184 available organic C and N stimulates microbial decomposition of soil organic matter in
- 1185 arctic permafrost soil, *Soil Biol. Biochem.*, doi:10.1016/j.soilbio.2014.04.014, 2014.
- 1186 Wild, B., Gentsch, N., Capek, P., Diáková, K., Alves, R. J. E., Bárta, J., Gittel, A., Hugelius, G.,
- 1187 Knoltsch, A., Kuhry, P., Lashchinskiy, N., Mikutta, R., Palmtag, J., Schleper, C., Schnecker, J.,
- 1188 Shibistova, O., Takriti, M., Torsvik, V. L., Urich, T., Watzka, M., Šantrůčková, H.,
- 1189 Guggenberger, G. and Richter, A.: Plant-derived compounds stimulate the decomposition
- 1190 of organic matter in arctic permafrost soils, *Sci. Rep.*, doi:10.1038/srep25607, 2016.
- 1191 Woods, G. C., Simpson, M. J., Pautler, B. G., Lamoureux, S. F., Lafrenière, M. J. and Simpson,
- 1192 A. J.: Evidence for the enhanced lability of dissolved organic matter following permafrost
- 1193 slope disturbance in the Canadian High Arctic, *Geochim. Cosmochim. Acta*,
- 1194 doi:10.1016/j.gca.2011.08.013, 2011.
- 1195 Wu, Y., Clarke, N. and Mulder, J.: Dissolved organic carbon concentrations in throughfall
- 1196 and soil waters at level II monitoring plots in norway: Short- and long-term variations,
- 1197 *Water. Air. Soil Pollut.*, doi:10.1007/s11270-009-0073-1, 2010.
- 1198 Xue, K.: Tundra soil carbon is vulnerable to rapid microbial decomposition under
- 1199 climatewarming, *Nat. Clim. Chang.*, doi:10.1038/NCLIMATE2940, 2017.
- 1200 Ye, B., Yang, D., Zhang, Z. and Kane, D. L.: Variation of hydrological regime with
- 1201 permafrost coverage over Lena Basin in Siberia, *J. Geophys. Res. Atmos.*,
- 1202 doi:10.1029/2008JD010537, 2009.
- 1203 Yu, Z.: Holocene carbon flux histories of the world's peatlands: Global carbon-cycle
- 1204 implications, *Holocene*, doi:10.1177/0959683610386982, 2011.
- 1205 Yue, C., Ciais, P., Zhu, D., Wang, T., Peng, S. S. and Piao, S. L.: How have past fire
- 1206 disturbances contributed to the current carbon balance of boreal ecosystems?,
- 1207 *Biogeosciences*, doi:10.5194/bg-13-675-2016, 2016.
- 1208 Zhang, K., Kimball, J. S., Mu, Q., Jones, L. A., Goetz, S. J. and Running, S. W.: Satellite based
- 1209 analysis of northern ET trends and associated changes in the regional water balance
- 1210 from 1983 to 2005, *J. Hydrol.*, doi:10.1016/j.jhydrol.2009.09.047, 2009.
- 1211 Zhang, X., Hutchings, J. A., Bianchi, T. S., Liu, Y., Arellano, A. R. and Schuur, E. A. G.:
- 1212 Importance of lateral flux and its percolation depth on organic carbon export in Arctic
- 1213 tundra soil: Implications from a soil leaching experiment, *J. Geophys. Res.*



1214 Biogeosciences, doi:10.1002/2016JG003754, 2017.
 1215 Zhu, D., Peng, S., Ciais, P., Zech, R., Krinner, G., Zimov, S. and Grosse, G.: Simulating soil
 1216 organic carbon in yedoma deposits during the Last Glacial Maximum in a land surface
 1217 model, Geophys. Res. Lett., doi:10.1002/2016GL068874, 2016.
 1218 Zubrzycki, S., Kutzbach, L., Grosse, G. and Desyatkin, A.: Organic carbon and total
 1219 nitrogen stocks in soils of the Lena River Delta, Biogeosciences, doi:10.5194/bg-10-
 1220 3507-2013, 2013.

1222 **Tables and Figures:**

1224 **Table 1:** Data type, name and sources of data files used to drive the model in the study
 1225 simulations.

Data Type	Name	Source
Vegetation Map	ESA CCI Land Cover Map	Bontemps et al., 2013
Topographic Index	STN-30p	Vörösmarty et al., 2000
Stream flow direction	STN-30p	Vörösmarty et al., 2000
River surface area		Lauerwald et al., 2015
Soil texture class		Reynolds et al. 1999
Climatology	GSWP3 v0, 1 degree	http://hydro.iis.u-tokyo.ac.jp/GSWP3/
Potential floodplains	Multi-source global wetland maps	Tootchi et al., 2018
Poor soils	Harmonized World Soil Database map	Nachtergaele et al., 2010
Spinup Soil Carbon Stock	20ky ORCHIDEE-MICT soil carbon spinup	Based on config. in Guimberteau et al. (2018)

1227
 1228
 1229

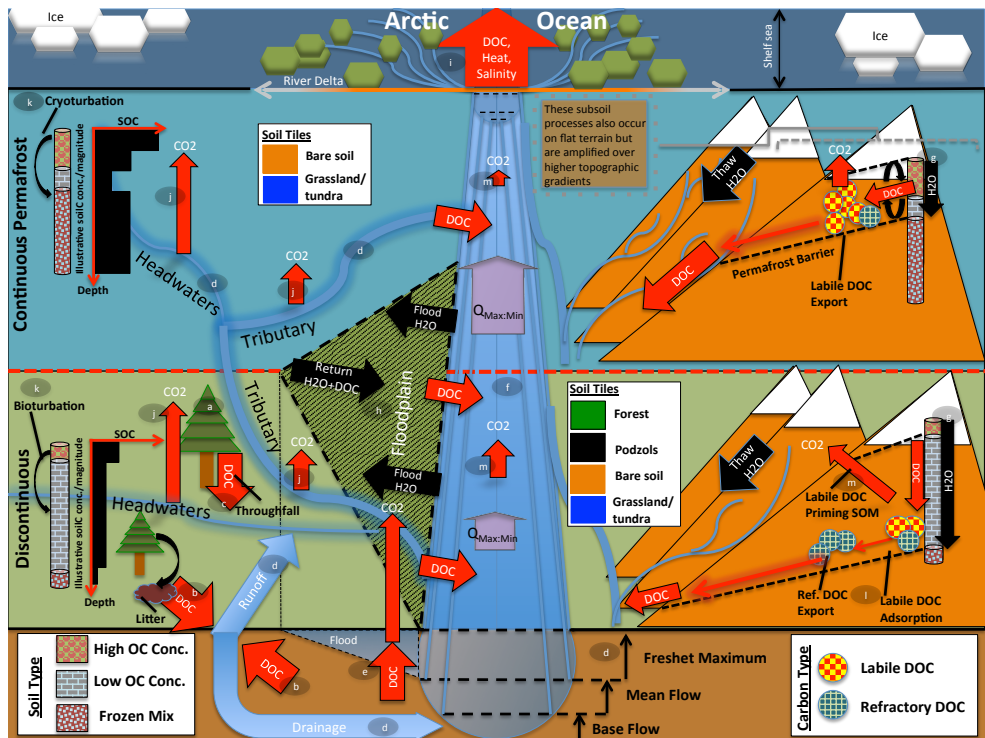
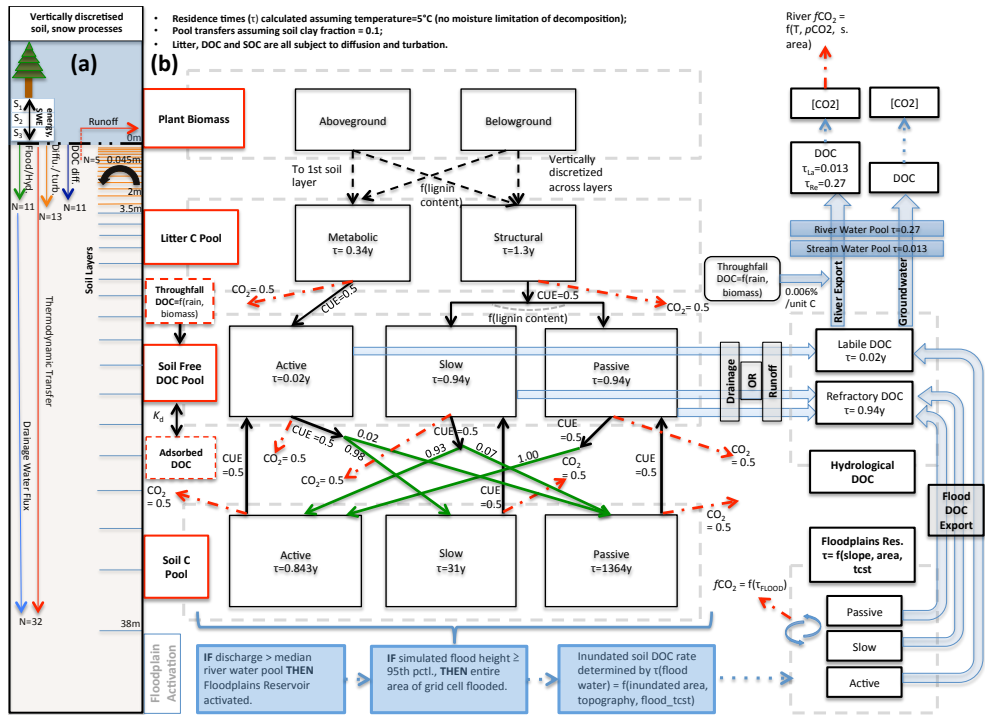


Figure 1: Cartoon diagram illustrating the landscape-scale emergent phenomena observed in high-latitude river systems that are captured by the processes represented in this model. Here, the terrestrial area is shown, in vertically-ascending order, as subsoil, discontinuous permafrost, continuous permafrost and the maritime boundary. Representative soil types, their distributions and carbon concentrations are shown for the two permafrost zones, as well as the different dynamics occurring on ‘flat’ (left) and ‘sloping’ land (right) arising from their permafrost designation. Carbon exports from one subsystem to another are shown in red. The relative strength of the same processes occurring in each permafrost band are indicated by relative arrow size. Note that the high CO₂ evasion in headwaters versus tributaries versus mainstem is shown here. Proposed and modelled mechanisms of soil carbon priming, adsorption and rapid metabolism are shown. The arrows $Q_{Max:Min}$ refer to the ratio of maximum to minimum discharge at a given point in the river, the ratio indicating hydrologic volatility, whose magnitude is influenced by permafrost coverage. Soil tiles, a model construct used for modulating soil permeability and implicit/explicit decomposition, are shown to indicate the potential differences in these dynamics for the relevant permafrost zones. Note that the marine shelf sea system, as shown in the uppermost rectangle, is not simulated in this model, although our outputs can be coupled for that purpose. Letter markings mark processes of carbon flux in permafrost regions and implicitly or explicitly included in the model, and can be referred to in subsections of the Methods text. These refer to: (a) Biomass generation; (b) DOC generation and leaching; (c) Throughfall and its DOC; (d) Hydrological mobilisation of soil DOC; (e) Soil flooding; (f) Landscape routing of water and carbon; (g) Infiltration and topography; (h)



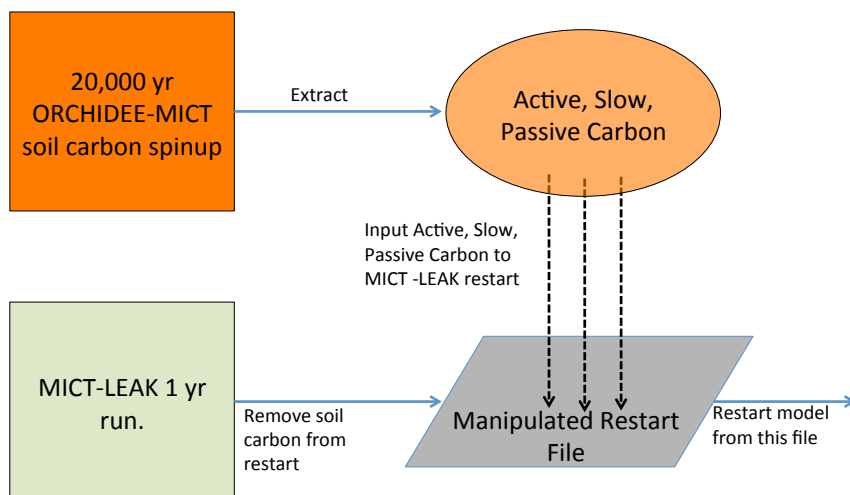
1256 Floodplain representation; (i) Oceanic outflow; (j) Dissolved carbon export and riverine
1257 atmospheric evasion; (k) Turbation; (l) Adsorption; (m) Priming.
1258
1259



1260
1261
1262
1263 **Figure 2** :Carbon and water flux map for core DOC elements in model structure relating
1264 to DOC transport and transformation. **(a)** Summary of the differing extent of vertical
1265 discretisation of soil and snow for different processes calculated in the model.
1266 Discretisation occurs along 32 layers whose thickness increases geometrically from 0-
1267 38m. N refers to the number of layers, SWE=snow water equivalent, S_n = Snow layer n.
1268 Orange layers indicate the depth to which diffusive carbon (turbation) fluxes occur. **(b)**
1269 Conceptual map of the production, transfer and transformation of carbon in its vertical
1270 and lateral (i.e., hydrological) flux as calculated in the model. Red boxes indicate meta-
1271 reservoirs of carbon, black boxes the actual pools as they exist in the model. Black
1272 arrows indicate carbon fluxes between pools, dashed red arrows give carbon loss as CO_2 ,
1273 green arrows highlight the fractional distribution of DOC to SOC (no carbon loss
1274 incurred in this transfer), a feature of this model. For a given temperature ($5^\circ C$) and soil
1275 clay fraction, the fractional fluxes between pools are given for each flux, while residence
1276 times for each pool (τ) are in each box. The association of carbon dynamics with the
1277 hydrological module are shown by the blue arrows. Blue dashed boxes illustrate the
1278 statistical sequence which activates the boolean floodplains module. Note that for
1279 readability, the generation and lateral flux of dissolved CO_2 is omitted from this diagram,
1280 but is described at length in the Methods section.



1281



1282

1283

1284

Figure 3: Flow diagram illustrating the step-wise stages required to implement the model's soil carbon stock prior to conducting transient, historical simulations.